Novel topological black holes from thermodynamics and deforming horizons

Jinbo Yang [*]

Department of Astronomy, School of Physics and Materials Science, Guangzhou University, Guangzhou 510006, People's Republic of China

(Received 18 January 2024; accepted 7 March 2024; published 15 April 2024)

Two novel topological black hole exact solutions with unusual shapes of horizons in the simplest holographic axions model, the four-dimensional Einstein-Maxwell-axions theory, are constructed. We draw embedding diagrams in various situations to display unusual shapes of novel black holes. To understand their thermodynamics from the quasilocal aspect, we rederive the unified first law and the Misner-Sharp mass from the Einstein equation for the spacetime as a warped product $\bar{\mathcal{M}}_{(2)} \times \hat{\mathcal{M}}_{(D-2)}$. The Ricci scalar $\hat{R}$ of the submanifold $\hat{\mathcal{M}}_{(D-2)}$ can be a nonconstant. We further improve the thermodynamics method based on the unified first law. Such a method simplifies constructing solutions and hints at generalization to higher dimensions. Moreover, we apply the unified first law to discuss black hole thermodynamics.

DOI: 10.1103/PhysRevD.109.084032

I. INTRODUCTION

Black hole physics, especially black hole thermodynamics, has brought us deep insights into theoretical physics [1–9]. The widely studied shape of the black hole has a spherical topology, supported by the topological theorem for Einstein gravity [10]. According to the theorem, the horizon of a four-dimensional asymptotically flat black hole must be topologically spherical. Nevertheless, many black objects beyond the spherical horizon in higher-dimensional supergravity or string theory have been discovered [11–16]. One kind of them is the topological black hole in asymptotic anti–de Sitter (AdS) space. Its horizon shape is not a sphere, but rather an Einstein manifold [17–20]. Widely studied topological black holes have planar or hyperbolic horizons [21–23]. The hyperbolic black hole can be viewed as a gravitational description of S-brane in string theory [24–26]. As for planar black holes, early relevant works should be dated back to Refs. [27,28]. They are widely applied in the context of AdS/CFT duality [29,30]. A planar nonextreme black hole in the AdS background corresponds to a specific boundary phase in finite temperature. Specifically, the so-called holographic axion model introduces various axions to achieve momentum relaxation, thus implying the finite dc conductivity on the boundary [31–39]. In such a model, the planar axionic black hole contains an axionic charge appearing in the first law of black hole thermodynamics [31,40]. The first law satisfies the Gibbs-Duhem relationship, hence it has Euler homogeneity.

The Gibbs-Duhem relationship satisfying the Euler homogeneity leads to some insights into the thermodynamics of topological black holes. Tian *et al.* first suggested to introduce the topological charge for a nonplanar Reissner-Nordström (RN) AdS black hole [41], which is discussed in detail in Ref. [42]. This topological charge has a similar scaling behavior to the axionic charge such that it preserves the Euler homogeneity. In recent years, Gao and co-workers have emphasized the importance of Euler homogeneity for understanding the black hole thermodynamics in a unified way with the usual thermodynamics [43–48]. They proposed the restricted phase space formalism and suggested introducing a "center charge" to the first law of black hole thermodynamics. Such a new thermodynamics quantity indicates degrees of freedom in some sense. It is similar to the color charge introduced by Visser in the context of extended phase space formalism [49]. These three distinct approaches, topological charge, color charge, and center charge, attach the same issue about adding new quantities to the first law of thermodynamics for topological black holes.

On the other hand, Einstein's gravity has a quasilocal mass called Misner-Sharp (MS) mass [50,51] for spherically symmetric spacetime due to the Kodama vector [52]. It reduces to the Arnowitt-Deser-Misner (ADM) mass when going to the spacelike infinity and the Bondi mass when going to the null infinity in the asymptotically flat background. Because of the quasilocal nature, the MS mass is widely applied in the context of primordial black hole formation [53–58], detailed study for Hawking

[*] yangjinbo@gzhu.edu.cn
Also at Institute for Theoretical Physics, Kanazawa University, Kanazawa 920-1192, Japan.
Also at HKUST Jockey Club Institute for Advanced Study, The Hong Kong University of Science and Technology, Clear Water Bay, Hong Kong, People's Republic of China.

evaporation [59–63], and P-V transition in cosmological background [64,65]. Moreover, the MS mass is significant for formulating the unified first law that unified the black hole thermodynamics and relativistic hydrodynamics [66]. References [67,68] further generalized the unified first law to discuss the thermodynamics of the apparent horizon (Hubble horizon) in an expanding universe and not limited to Einstein's gravity. These works also inspire a novel approach to generate spherical black hole solutions of general relativity from thermodynamics [69], later developed in Refs. [70–74], including planar and hyperbolic cases in or not in the context of modified gravity.

This article explores the possibility of replacing the spherical part with an unusual shape, not limited to maximally symmetric space or Einstein manifold. Suppose the part replacing the sphere is an independent manifold with metric $\hat{g}_{ij}(x)$, where x denotes the point in the independent manifold, and i, j, k are the corresponding indexes. If the manifold is maximally symmetric, the Riemann tensor from $\hat{g}_{ij}(x)$ is

$$\hat{R}_{ijkl} = k(\hat{g}_{ik}\hat{g}_{jl} - \hat{g}_{il}\hat{g}_{jk}), \tag{1.1}$$

where $k = 1$ is for sphere, $k = 0$ is for plane, and $k = -1$ is for hyperbolic surface. Furthermore, an Einstein manifold satisfies a weaker condition

$$\hat{R}_{ij}(x) = \lambda\hat{g}_{ij}(x), \tag{1.2}$$

where λ is a constant [18]. Hence, the Ricci scalar $\hat{R}$ is also a constant. Although cases about nonconstant curvature are discussed in the context of modified gravity [75–78], it is long believed that general relativity demands an Einstein manifold. We will show that the simplest holographic axion model contains black hole solutions with unusual shapes of horizons. The spacetime is still a warped product, but the transverse space is not an Einstein manifold and its $\hat{R}$ can depend on direction x.

In addition, we will generalize the unified first law to these nonconstant $\hat{R}$ cases. This implies an efficient method for constructing exact solutions inspired by Refs. [69,71–73,79,80]. We call it the thermodynamics method and use it to justify the *Ansätze* for obtaining novel solutions. The method simply induces the constraint equation for $\hat{g}_{ij}(x)$. Moreover, the unified first law provides a quasilocal viewpoint to understand the first law of black hole thermodynamics even without precise definitions of global parameters. It is beneficial to deal with those black hole solutions.

The article is organized as follows. In Sec. II, we will introduce the action of the simplest holographic axion model in $D = 4$ and give two novel charged topological black hole solutions. The crucial feature is that the intrinsic metric of the transverse space can have a nonconstant Ricci scalar, different from topological RN black holes without axion or planar axionic black holes. We will draw embedding diagrams to visualize the shapes of horizons for various situations. In Sec. III, we will rederive the unified first law of general relativity from the Einstein equation and give an improved thermodynamics method proposed in Ref. [69] originally. Such a method simplifies solving the Einstein equation and hence hints at generalizing the novel solutions. We will also apply the quasilocal viewpoint offered by the unified first law to discuss the first law of thermodynamics for these deformed topological black holes. Section IV will give a conclusive summary.

II. ACTION AND SOLUTIONS

We consider the following action:

$$S = \int d^4x\sqrt{-g}\bigg(\frac{1}{16\pi G_N}(R - 2\Lambda) - \frac{1}{16\pi}F^{\mu\nu}F_{\mu\nu} - \frac{1}{2}g^{\mu\nu}\partial_\mu\psi^I\partial_\nu\psi^I\bigg), \tag{2.1}$$

where $F_{\mu\nu} = \partial_\mu A_\nu - \partial_\nu A_\mu$ is the strength of the $U(1)$ gauge field A_μ and ψ^I with $I = 1, 2$ are two massless scalars. The equations of motion are

$$R_{\mu\nu} - \frac{1}{2}Rg_{\mu\nu} + \Lambda g_{\mu\nu} = 8\pi G_N({T^{(em)}}_{\mu\nu} + {T^{(\psi)}}_{\mu\nu}), \tag{2.2}$$

$$\nabla_\mu F^{\mu\nu} = \frac{1}{\sqrt{-g}}\frac{\partial}{\partial x^\mu}(\sqrt{-g}F^{\mu\nu}) = 0, \tag{2.3}$$

$$\nabla^\mu\nabla_\mu\psi^I = \frac{1}{\sqrt{-g}}\frac{\partial}{\partial x^\mu}\left(\sqrt{-g}g^{\mu\nu}\frac{\partial\psi^I}{\partial x^\nu}\right) = 0, \tag{2.4}$$

where

$${T^{(em)}}_{\mu\nu} = \frac{1}{4\pi}\left(F_{\mu\alpha}{F_\nu}^\alpha - \frac{1}{4}F_{\alpha\beta}F^{\alpha\beta}g_{\mu\nu}\right), \tag{2.5}$$

$${T^{(\psi)}}_{\mu\nu} = \partial_\mu\psi^I\partial_\nu\psi^I - \frac{1}{2}g_{\mu\nu}g^{\lambda\sigma}\partial_\lambda\psi^I\partial_\sigma\psi^I. \tag{2.6}$$

Equation (2.2) is the Einstein equation with the energy-momentum tensor (2.5) (for electromagnetic field) and (2.6) (for axions). Equation (2.3) is the Maxwell equation and Eq. (2.4) is the free Klein-Gordon (KG) equations for axions. This theory is the same as the four-dimensional case of the holographic model proposed by Ref. [31], which aims to achieve momentum relaxation. Their model considered $(d + 1)$-dimensional spacetime and introduced $d - 1$ massless scalars. The action thus has global shift symmetries, i.e., invariant under transformation

$$\psi^I \to \psi^I + c^I. \tag{2.7}$$

Hence, scalars ψ^I are usually viewed as axions. Later extended studies are called holographic axion models, which introduce axions to deduce the momentum relaxation, then obtain a finite dc conductivity for the strong coupling theory living on the boundary of AdS spacetime (Ref. [31]). Distinguished with the interest of beyond the standard model, holographic axion models usually do not introduce the coupling of axions ψ^I and topological term $F \wedge F$. Relevant investigations are well summarized in Ref. [38].

A. Solution I

The next task is to solve those equations of motion. We take the *Ansatz* as

$$ds^2 = -f(r)dt^2 + \frac{dr^2}{f(r)} + r^2\left(\frac{d\rho^2}{1-k\rho^2-e(\rho)} + \rho^2 d\varphi^2\right),$$
$$A_\mu dx^\mu = -\phi(r)dt, \quad \psi^1(\rho) = \alpha p(\rho), \quad \psi^2(\varphi) = \alpha\varphi. \tag{2.8}$$

The *Ansatz* for $\psi^2(\varphi)$ solves Eq. (2.4) in which $I = 2$, while Eq. (2.2) gives

$$k - f - r\frac{df}{dr} - \Lambda r^2 - G_N\left(\frac{d\phi}{dr}\right)^2 = -\frac{1}{2\rho}\frac{de}{d\rho} + \frac{4\pi G_N \alpha^2}{\rho^2}\left(1 + \rho^2(1-k\rho^2-e)\left(\frac{dp}{d\rho}\right)^2\right), \tag{2.9}$$

$$\frac{1}{2}\frac{d^2 f}{dr^2} + \frac{1}{r}\frac{df}{dr} + \Lambda = G_N\left(\frac{d\phi}{dr}\right)^2, \tag{2.10}$$

$$\rho^2(1-k\rho^2-e)\left(\frac{dp}{d\rho}\right)^2 - 1 = 0. \tag{2.11}$$

The last equation leads to

$$\frac{dp}{d\rho} = \pm\frac{1}{\rho\sqrt{1-k\rho^2-e}}. \tag{2.12}$$

Then it solved Eq. (2.4) in which $I = 1$. This is because the *Ansatz* $\psi^1(\rho) = \alpha p(\rho)$ implies

$$\frac{d}{d\rho}\left(\rho(1-k\rho^2-e)\frac{dp}{d\rho}\right) + \frac{1}{2}\rho\left(2k\rho + \frac{de}{d\rho}\right)\frac{dp}{d\rho} = 0. \tag{2.13}$$

Furthermore, Eq. (2.3) leads to

$$\frac{d^2\phi}{dr^2} + \frac{2}{r}\frac{d\phi}{dr} = 0, \tag{2.14}$$

such that it determines the electric potential as

$$\phi = \frac{4\pi Q}{\Omega r}, \tag{2.15}$$

up to some freedom for gauge fixing. We have used Ω to donate the size of the unit surface $\mathcal{S}$ in the transverse space in which we are interested. It is an area integral

$$\Omega = \int_{\mathcal{S}} \frac{\rho}{\sqrt{1-k\rho^2-e}} d\rho d\varphi. \tag{2.16}$$

The $U(1)$ charge inside the region surrounded by such a surface is

$$Q = \frac{1}{4\pi}\int_{\mathcal{S}} *F = \int_{\mathcal{S}}\left(-\frac{d\phi}{dr}\right) r^2 \frac{\rho}{\sqrt{1-k\rho^2-e}} d\rho d\varphi. \tag{2.17}$$

Moreover, the solution (2.15) also implies that the derivative of Eq. (2.9) with respect to r gives Eq. (2.10). Noting that the left-hand side (lhs) of Eq. (2.9) only relates to r, while the right-hand side (rhs) of Eq. (2.9) only depends on ρ, Eq. (2.9) should be equal to a constant η. Namely,

$$\eta = k - f - r\frac{df}{dr} - \Lambda r^2 - \left(\frac{4\pi}{\Omega}\right)^2 \frac{G_N Q^2}{r^2}, \tag{2.18}$$

$$\eta = -\frac{1}{2\rho}\frac{de}{d\rho} + \frac{8\pi G_N \alpha^2}{\rho^2}, \tag{2.19}$$

in which the solution (2.12) is substituted. One can introduce $c = k - \eta$ to solve Eq. (2.18). As for Eq. (2.19), this equation is solved by

$$e(\rho) = -\eta\rho^2 + 16\pi G_N \alpha^2 \log(\beta\rho). \tag{2.20}$$

Thus, η contributes a $-\eta\rho^2$ term to $e(\rho)$. It hence shifts the $-k\rho^2$ as $-c\rho^2$ in $p(\rho)$ and the metric. In summary, the full solution is given by

$$ds^2 = -\left(c - \frac{8\pi G_N M}{\Omega r} + \left(\frac{4\pi}{\Omega}\right)^2 \frac{G_N Q^2}{r^2} - \frac{\Lambda r^2}{3}\right) dt^2 + \left(c - \frac{8\pi G_N M}{\Omega r} + \left(\frac{4\pi}{\Omega}\right)^2 \frac{G_N Q^2}{r^2} - \frac{\Lambda r^2}{3}\right)^{-1} dr^2 + r^2\left(\frac{d\rho^2}{1 - c\rho^2 - 16\pi G_N \alpha^2 \log(\beta\rho)} + \rho^2 d\varphi^2\right),$$
$$A_\mu dx^\mu = -\phi(r)dt = -\frac{4\pi Q}{\Omega r}dt,$$
$$\psi^1 = \alpha\int^\rho \frac{d\tilde{\rho}}{\tilde{\rho}\sqrt{1 - c\tilde{\rho}^2 - 16\pi G_N \alpha^2 \log(\beta\tilde{\rho})}},$$
$$\psi^2 = \alpha\varphi. \tag{2.21}$$

1. Compare with topological RN-(A)dS black holes

The solution (2.21) reduces to three kinds of topological RN black holes up to some scaling of ρ by setting $\alpha = 0$ and identifying φ with $\varphi + 2\pi$. This is because $c = k$ in these cases. Then positive c corresponds the zero genus ($g = 0$); $c = 0$ is for $g = 1$; the negative c is for higher genus $g > 1$, see Refs. [12,81]. Meanwhile, such a period condition for φ forces the field space to have a cylinder topology though the field space metric δ_{IJ} is flat. If $\alpha \neq 0$, the transverse space is still different from those previously studied topological black holes even when r tends to infinity. In the case of $\Lambda = 0$ and positive c, the metric in (2.21) is certainly not an asymptotically flat spacetime. Such a property is similar to the global monopole spacetime, which is not asymptotically flat, since it has a deficit angle at r infinity. Even when $\Lambda \neq 0$, it seems inappropriate to treat the metric as an asymptotical (A)dS geometry due to the deformed shapes of the transverse space.

On the other hand, the t-r part of the metric in Eq. (2.21) is similar to the t-r metric for topological RN solutions even though $\alpha \neq 0$. Hence, the parameter space for the metric should include the naked singularity and the extreme black hole. We do not discuss these cases in the following, but instead, we are interested in nonextreme black holes. For situations of $\Lambda \leq 0$, we will work in the parameter regions of the equation $f(r) = 0$ containing two different positive roots. The larger one indicates the black hole horizon location, while the smaller one corresponds to the inner Cauchy horizon. As for $\Lambda > 0$, the equation $f(r) = 0$ may have three positive roots. The largest one should be the cosmic horizon rather than the black hole horizon.

We plot typical cases for nonextreme black holes in Figs. 1–3. For simplicity, we set

$$r_g = 8\pi G_N M/\Omega, \tag{2.22}$$

as the unit for the r coordinate, and choose the value of Q by requiring

$$G_N(4\pi Q/\Omega)^2 = 0.09 r_g^2. \tag{2.23}$$

The value of Λ is taken as 0 in Fig. 1, $0.09 r_g^{-2}$ in Fig. 2, and $-0.09 r_g^{-2}$ in Fig. 3. It is worth noting that the black hole

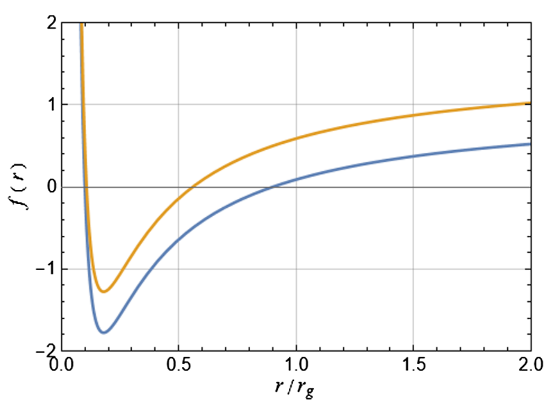

FIG. 1. We set $r_g = 8\pi G_N M/\Omega$ and $G_N(4\pi Q/\Omega)^2 = 0.09 r_g^2$ to plot $f(r) = c - (8\pi G_N M/\Omega)/r + G_N(4\pi Q/\Omega)^2/r^2$. The blue curve represents $f(r)$ when $c = 1$. It has roots $r = 0.9 r_g$ indicating the black hole horizon location, and $r = 0.1 r_g$ corresponding to the inner Cauchy horizon; whereas the yellow curve is for the $c = 1.5$ case, which has roots $r = 0.5594 r_g$ (black hole horizon) and $r = 0.1073 r_g$ (inner horizon).

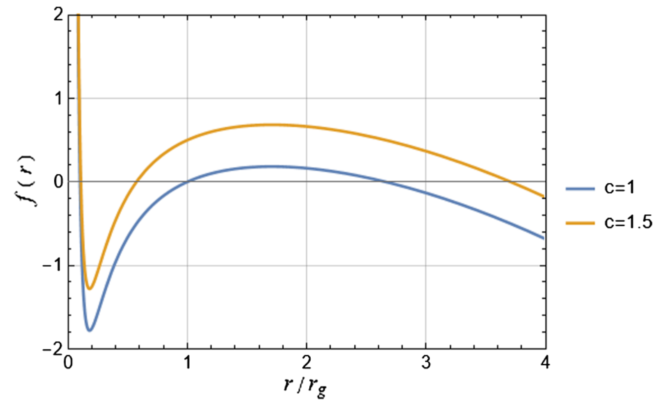

FIG. 2. We set $G_N(4\pi Q/\Omega)^2 = 0.09 r_g^2$ and $\Lambda = 0.09 r_g^{-2}$ to plot $f(r) = c - (8\pi G_N M/\Omega)/r + G_N(4\pi Q/\Omega)^2/r^2 - \Lambda r^2/3$ in which $r_g = 8\pi G_N M/\Omega$ is the unit of r. The blue curve is for the $c = 1$ case. The largest root of $f(r) = 0$ is $r = 2.660 r_g$, which represents the cosmic horizon, whereas other two roots are $r = 1.000 r_g$ (black hole horizon) and $r = 0.1000 r_g$ (inner horizon). As for the yellow curve, the case of $c = 1.5$, roots are $r = 3.707 r_g$ (cosmic horizon), $r = 0.5733 r_g$ (black hole horizon), and $r = 0.1072 r_g$ (inner horizon).

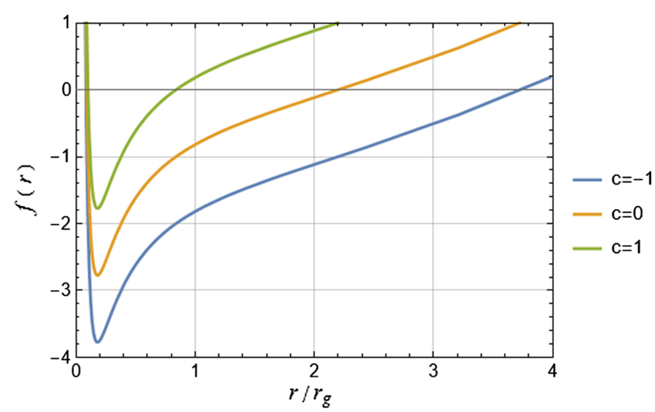

FIG. 3. We set $G_N(4\pi Q/\Omega)^2 = 0.09 r_g^2$ and $\Lambda = -0.09 r_g^{-2}$ to plot $f(r) = c - (8\pi G_N M/\Omega)/r + G_N(4\pi Q/\Omega)^2/r^2 - \Lambda r^2/3$ in which $r_g = 8\pi G_N M/\Omega$. The blue curve is for $c = -1$. Roots of $f(r) = 0$ are $r = 3.743 r_g$ (black hole horizon) and $r = 0.08310 r_g$ (inner horizon). The yellow curve is for $c = 0$ with roots $r = 2.201 r_g$ (black hole horizon) and $r = 0.09001 r_g$ (inner horizon). The green curve is for $c = 1$ with roots $r_H = 0.8395 r_g$ (black hole horizon) and $r = 0.1000 r_g$ (inner horizon).

horizon $r = r_H$ should satisfy $f(r_H) = 0$ and $f'(r_H) > 0$. While other roots r_C of $f(r) = 0$ with negative $f'(r_C)$ should be an inner Cauchy horizon or a cosmic horizon. When $\Lambda \geq 0$ and $c \leq 0$, only the horizon with negative f' exists. Nevertheless, cases of $\Lambda < 0$ and $c \leq 0$ always include a black hole horizon (see Fig. 3).

2. Shapes of horizons

Then we will study the geometry of the transverse space, which is labeled as $\hat{\mathcal{M}}_2$. Its independent line element $d\hat{s}^2 = \hat{g}_{ij} dx^i dx^j$ seems described by three parameters c, α, and β, but one of them can be set to 1 via a suitable rescaling. We choose

$$\begin{aligned} \tilde{\rho} &= \beta\rho, & \tilde{r} &= r/\beta, & \tilde{t} &= \beta t, \\ \tilde{c} &= c/\beta^2, & \tilde{M} &= M/\beta^3, & \tilde{Q} &= Q/\beta^2, \end{aligned} \tag{2.24}$$

then obtain the line element for the whole spacetime,

$$\begin{aligned} ds^2 = &-\left(\tilde{c} - \frac{8\pi G_N \tilde{M}}{\Omega \tilde{r}} + \left(\frac{4\pi}{\Omega}\right)^2 \frac{G_N \tilde{Q}^2}{\tilde{r}^2} - \frac{\Lambda \tilde{r}^2}{3}\right) d\tilde{t}^2 \\ &+ \left(\tilde{c} - \frac{8\pi G_N \tilde{M}}{\Omega \tilde{r}} + \left(\frac{4\pi}{\Omega}\right)^2 \frac{G_N \tilde{Q}^2}{\tilde{r}^2} - \frac{\Lambda \tilde{r}^2}{3}\right)^{-1} d\tilde{r}^2 \\ &+ \tilde{r}^2 \left(\frac{d\tilde{\rho}^2}{1 - c\tilde{\rho}^2 - 16\pi G_N \alpha^2 \log(\tilde{\rho})} + \tilde{\rho}^2 d\varphi^2\right). \end{aligned} \tag{2.25}$$

Particularly, when we omit the tilde sign, we have the line element of $\hat{\mathcal{M}}_2$,

$$d\hat{s}^2 = \frac{d\rho^2}{1 - c\rho^2 - 16\pi G_N \alpha^2 \log\rho} + \rho^2 d\varphi^2. \tag{2.26}$$

Therefore, the Ricci scalar of $\hat{\mathcal{M}}_2$ is

$$\hat{R}(\rho) = 2c + \frac{16\pi G_N \alpha^2}{\rho^2}, \tag{2.27}$$

which depends on the value of ρ rather than a constant. The intrinsic geometry of $\hat{\mathcal{M}}_2$ is controlled by two parameters c and α; α contributes the ρ dependence and probably leads to a singularity $\rho = 0$. It would be interesting to study the consequence of the existence of a singular direction for quantum gravity, though the entropy of the horizon with arbitrary shape is studied in a quantum gravity context [82].

On the other hand, $\hat{g}_{\rho\rho}$ should be positive to ensure the correct signature of the metric, such that

$$c < \frac{1 - 16\pi G_N \alpha^2 \log\rho}{\rho^2}. \tag{2.28}$$

The rhs of the above inequality as a function of ρ takes the minimum

$$c_{\text{crit}} = -8\pi G_N \alpha^2 \exp\left(-1 - \frac{1}{8\pi G_N \alpha^2}\right), \tag{2.29}$$

at the location

$$\rho_{\min} = \exp\left(\frac{1}{2} + \frac{1}{16\pi G_N \alpha^2}\right). \tag{2.30}$$

Thus, any smaller c never intersects with the function $(1 - 16\pi G_N \alpha^2 \log\rho)/\rho^2$. We take $16\pi G_N \alpha^2 = 10$ to plot this function in Fig. 4. It shows that a positive c intersects with the function (blue) only once, while a negative c, but larger than -1.506, intersects twice. For instance, the case of $c = -1$ (yellow) has two branches satisfying the inequality (2.28). One is $0 < \rho < 1.313$, called the small branch, while another is the large branch $\rho > 3.314$. It is worth noting that $\rho = 1.313$ and $\rho = 3.314$ indicate somewhere the $\hat{g}_{\rho\rho}$ blows up. Generally, the roots of

$$\frac{1}{\hat{g}_{\rho\rho}} = 1 - c\rho^2 - 16\pi G_N \alpha^2 \log\rho = 0 \tag{2.31}$$

serve as coordinate singularities that can be removed by choosing a new coordinate,

$$l = \int \sqrt{\hat{g}_{\rho\rho}(\rho)}\, d\rho. \tag{2.32}$$

The line element under the new coordinates $\{l, \varphi\}$ is

$$d\hat{s}^2 = dl^2 + \rho^2(l) d\varphi^2. \tag{2.33}$$

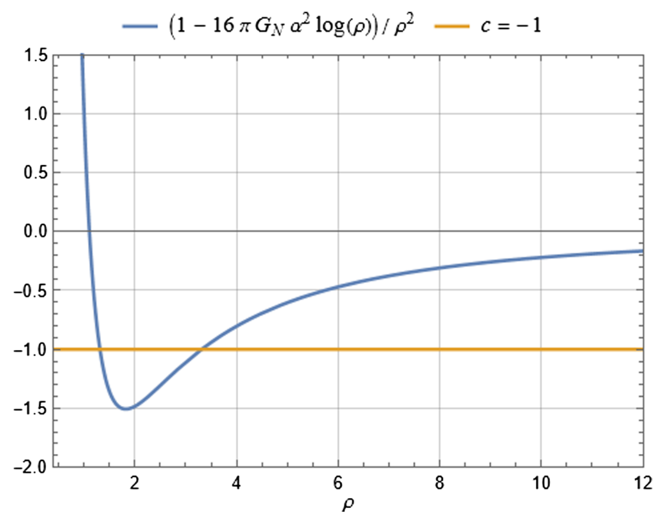

FIG. 4. The blue curve describes the function $(1 - 16\pi G_N \alpha^2 \log\rho)/\rho^2$ when $16\pi G_N \alpha^2$ is taken as 10. It has a minimum value -1.506 at $\rho = 1.822$. The yellow line $c = -1$ intersects the function at $\rho = 1.313$ and $\rho = 3.314$. Hence, we obtain a small branch $0 < \rho < 1.313$ and a large branch $\rho > 3.314$ to ensure $c < (1 - 16\pi G_N \alpha^2 \log\rho)/\rho^2$, namely, a positive $\hat{g}_{\rho\rho}$.

Thus, roots of $1/\hat{g}_{\rho\rho}$ are somewhere satisfied $d\rho/dl = 0$, indicating the minimum or maximum of ρ. The integral (2.32) will introduce an integral constant. We determine such a constant by requiring $l = 0$ when ρ becomes the minimum or maximum.

Then we will draw embedded diagrams for several situations to visualize the $\hat{\mathcal{M}}_2$ geometry. First, we rewrite the line element (2.26) as

$$d\hat{s}^2 = \frac{c\rho^2 + 16\pi G_N\alpha^2 \log\rho}{1 - c\rho^2 - 16\pi G_N\alpha^2 \log\rho} d\rho^2 + d\rho^2 + \rho^2 d\varphi^2, \quad (2.34)$$

which hints at how to embed $\hat{\mathcal{M}}_2$ into a three-dimensional flat space. If

$$\hat{g}_{\rho\rho} - 1 = \frac{c\rho^2 + 16\pi G_N\alpha^2 \log\rho}{1 - c\rho^2 - 16\pi G_N\alpha^2 \log\rho} \quad (2.35)$$

is positive, defining

$$z_{\mathrm{E}} = \int \sqrt{\hat{g}_{\rho\rho} - 1} d\rho \quad (2.36)$$

embeds the $\hat{g}_{\rho\rho} - 1 > 0$ part of $\hat{\mathcal{M}}_2$ into a Euclidean space. Whereas $\hat{g}_{\rho\rho} - 1 < 0$ should be embedded into a Minkowski space via

$$z_{\mathrm{M}} = \int \sqrt{1 - \hat{g}_{\rho\rho}} d\rho. \quad (2.37)$$

Therefore, it would be beneficial to discuss the sign of $\hat{g}_{\rho\rho} - 1$ before drawing the embedding diagram.

Let us refer back to the case of $c = -1$ and $16\pi G_N\alpha^2 = 10$. We plot the corresponding $\hat{g}_{\rho\rho} - 1$ in Fig. 5. The function $\hat{g}_{\rho\rho} - 1$ also blows up at $\rho = 1.313$ and $\rho = 3.314$, which indicates the range of ρ for the small branch and the large branch. $\hat{g}_{\rho\rho} - 1$ is negative in $0 < \rho < 1.138$ and positive in $1.138 < \rho < 1.313$ for the small branch; whereas for the large branch, $\hat{g}_{\rho\rho} - 1$ changes its sign at $\rho = 3.566$ from positive to negative.

For the small branch, the $0 < \rho < 1.313$ region should be embedded into an Euclidean space due to its positive $\hat{g}_{\rho\rho} - 1$. Such a shape is described by the left figure of Fig. 6. While the $1.138 < \rho < 1.313$ region of $\hat{\mathcal{M}}_2$ corresponds to the middle figure of Fig. 6. The right figure of Fig. 6 shows how to join these two parts together. Remembering the issue of coordinate singularity $1/\hat{g}_{\rho\rho} = 0$, we transform the coordinate ρ to l. The relation between ρ and l is described by the left plot in Fig. 7, in which we have set $l = 0$ at the maximum $\rho = 1.313$. The yellow curve describes another copy of the blue curve. Hence, they represent the full region for the function $\rho(l)$. The right figure of Fig. 7 is the embedding diagram for the whole $\hat{\mathcal{M}}_2$. There are two sharp peaks corresponding to

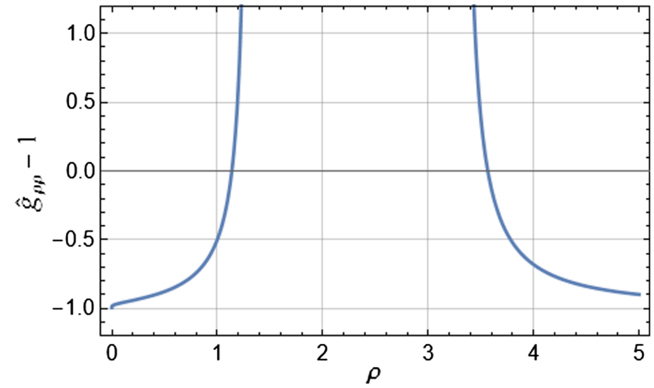

FIG. 5. Plot for $\hat{g}_{\rho\rho} - 1$ in the case of $c = -1$ of $16\pi G_N\alpha^2 = 10$: $\hat{g}_{\rho\rho} - 1$ changes its sign at $\rho = 1.138$ and $\rho = 3.566$. It also blows up at $\rho = 1.313$ and $\rho = 3.314$. Hence, the positive $\hat{g}_{\rho\rho} - 1$ regions are $1.138 < \rho < 1.313$ and $3.314 < \rho < 3.566$; hence they can be embedded into a three-dimensional flat Euclidean space. The regions $0 < \rho < 1.313$ and $\rho > 3.566$ can be embedded into a Minkowski space due to their negative $\hat{g}_{\rho\rho} - 1$.

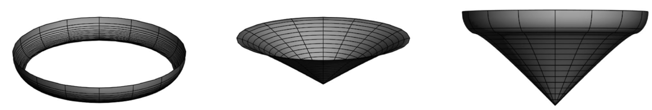

FIG. 6. The small branch for the case of $c = -1$ of $16\pi G_N\alpha^2 = 10$: The left figure corresponds to the $0 < \rho < 1.313$ region which is embedded into a Minkowski space; the middle one is for $1.138 < \rho < 1.313$ embedded in an Euclidean space; the right figure shows two regions joined together.

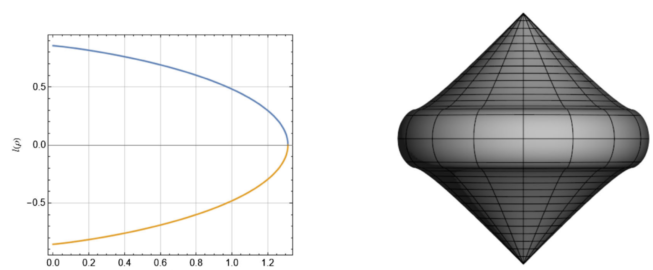

FIG. 7. The small branch for the case of $c = -1$ of $16\pi G_N\alpha^2 = 10$: The left figure shows the function $l(\rho)$ in which the yellow curve is for another copy. We set $l = 0$ at $\rho = 1.313$, i.e., the maximum of ρ. The right figure is the complete embedded diagram.

$\rho = 0$. They are intrinsic singularities because the independent Ricci scalar is divergent when ρ tends to 0.

The large branch is not singular since it starts from the minimum $\rho = 3.314$ and then excludes the singularity $\rho = 0$. The intrinsic Ricci scalar (2.27) thus has an upper bound. Similarly, the positive $\hat{g}_{\rho\rho} - 1$ region $3.314 < \rho < 3.566$ indicates that it can be embedded into a flat Euclidean space, as shown in the left figure of Fig. 8, whereas the middle one corresponds to the region $\rho > 3.566$ embedded into a Minkowski space. The right figure

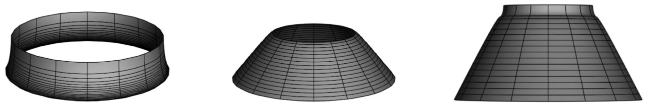

FIG. 8. The large branch for the case of $c = -1$ of $16\pi G_N \alpha^2 = 10$: The left figure corresponds to the $3.314 < \rho < 3.566$ region which is embedded into an Euclidean space; the middle one is for the $\rho > 3.566$ region embedded in a Minkowski space; the right figure shows two regions joined together.

of Fig. 8 shows the joined figure. Finally, we plot Fig. 9 to complete the embedding. The left figure shows the function $l(\rho)$ containing another copy (yellow) in which we have set $l = 0$ at the minimum $\rho = 3.314$. The right figure shows the entire embedding diagram. There are other interesting cases when keeping $16\pi G_N \alpha^2 = 10$. If c is smaller than the minimum value -1.5059, ρ runs from 0 to infinity without any point making $\hat{g}_{\rho\rho}$ blow up. We take $c = -1.6$ to plot $\hat{g}_{\rho\rho} - 1$ and draw the embedding diagram in Fig. 10. Depending on the sign of $\hat{g}_{\rho\rho} - 1$, the lower four figures from left to right correspond to (1) the $0 < \rho < 1.323$ region embedded into a Minkowski space, (2) the $1.323 < \rho < 2.253$ region embedded into an Euclidean space, (3) the $\rho > 2.253$ region embedded into a Minkowski space again, and (4) the whole $\rho > 0$ region, respectively. Furthermore, a more negative c may imply that no region can be embedded into an Euclidean flat space. For instance, the left plot of Fig. 11 shows the case of $c = -2$, which satisfies $0 < \hat{g}_{\rho\rho} < 1$ in the whole region of $\rho > 0$. Hence, $\hat{\mathcal{M}}_2$ in this case should be entirely embedded into a Minkowski space, as shown in the right figure of Fig. 11.

If we still use $16\pi G_N \alpha^2 = 10$, a non-negative c does not produce a new embedding diagram, but is still similar to the small branch for $c = -1$. They will have a very small maximum ρ. Instead, we take $c = 1$ and $16\pi G_N \alpha^2 = 0.1$ to show a case with positive c. The equation

$$1 - \rho^2 - 0.1 \log \rho = 0 \qquad (2.38)$$

has a root $\rho = 1$, so the range of ρ is $0 < \rho < 1$. The upper plot in Fig. 12 shows that $\hat{g}_{\rho\rho} - 1$ has a root $\rho = 0.3320$. Then the lower figures show several parts of the embedded diagram. The left plot describes the $0 < \rho < 0.3320$ region embedded in Euclidean space, the middle one describes the $0.3320 < \rho < 1$ region embedded in a Minkowski space, and the right one shows the joined embedding diagram. The left plot in Fig. 13 shows the numerical results of $l(\rho)$ in which $l = 0$ at the maximum $\rho = 1$. The yellow curve shows another copy. Then we obtain the whole embedding

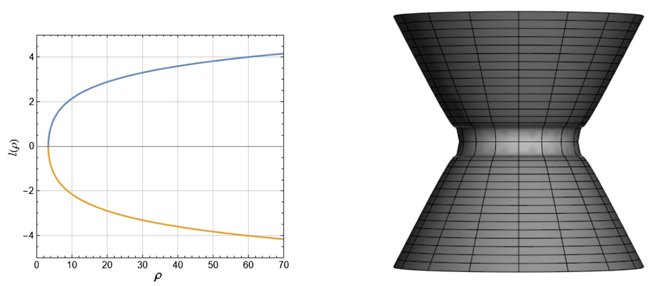

FIG. 9. The large branch for the case of $c = -1$ of $16\pi G_N \alpha^2 = 10$: The left figure shows the function $l(\rho)$ in which the yellow curve is for another copy. We set $l = 0$ at $\rho = 3.566$, i.e., the minimum of ρ. The right figure is the complete embedded diagram.

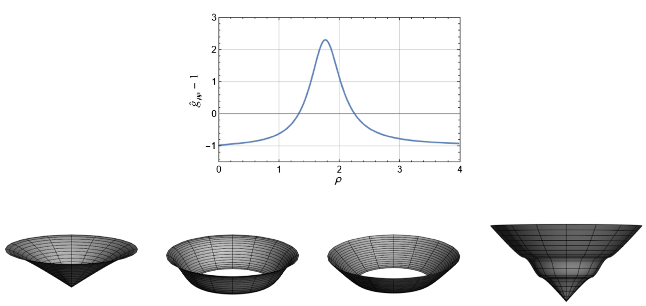

FIG. 10. The case of $c = -1.6$ and $16\pi G_N \alpha^2 = 10$: The upper plot shows that $\hat{g}_{\rho\rho} - 1$ is positive in $1.323 < \rho < 2.253$, but negative in $0 < \rho < 1.323$ and $\rho > 2.253$. The lower figures from left to right are (1) the $0 < \rho < 1.323$ region embedded into a Minkowski space; (2) the $1.323 < \rho < 2.253$ region embedded into an Euclidean space; (3) the $\rho > 2.253$ region embedded into a Minkowski space again; and (4) the whole $\rho > 0$ region, respectively.

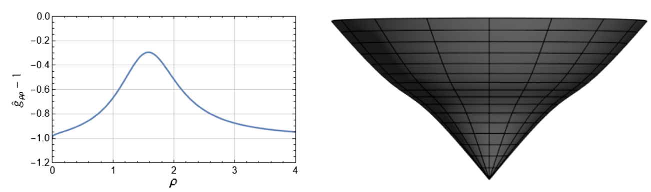

FIG. 11. The case of $c = -2$ and $16\pi G_N \alpha^2 = 10$: The left plot shows $\hat{g}_{\rho\rho} - 1 < 0$. Hence, the whole $\hat{\mathcal{M}}_2$ should be embedded into a Minkowski space, with the shape as the right figure shows.

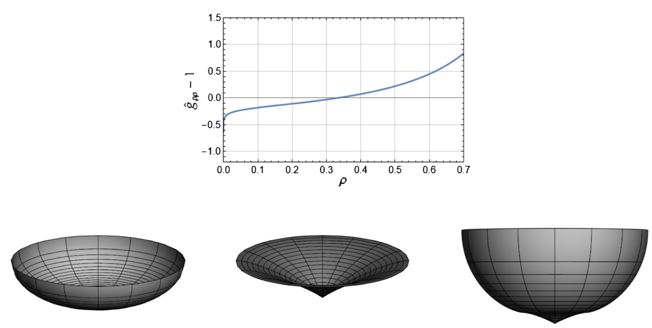

FIG. 12. The case of $c = 1$ and $16\pi G_N \alpha^2 = 0.1$: The upper plot shows $\hat{g}_{\rho\rho} - 1$ with a root $\rho = 0.3320$. The lower figures are embedded diagrams: the left figure is for $0.3320 < \rho < 1$ (Euclidean); the middle figure is for $0 < \rho < 0.3320$ (Minkowski); the right one is the joined figure.

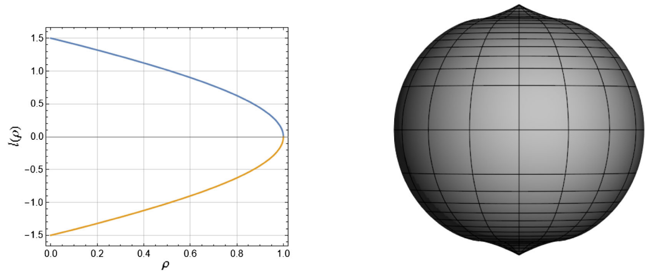

FIG. 13. The case of $c = 1$ and $16\pi G_N \alpha^2 = 0.1$: The left figure shows the function $l(\rho)$. We set $l = 0$ at $\rho = 1$, i.e., the maximum of ρ. The right figure is the complete embedded diagram.

diagram, the right figure in Fig. 13, which serves as a deformed sphere.

B. Solution II

There is an alternative *Ansatz* without posing period conditions in the field space. It is

$$ds^2 = -f(r)dt^2 + \frac{dr^2}{f(r)} + r^2 e^{\lambda(\rho)}(d\rho^2 + \rho^2 d\varphi^2),$$
$$A_\mu dx^\mu = -\phi(r)dt, \quad \psi^1 = \alpha\rho\cos\varphi, \quad \psi^2 = \alpha\rho\sin\varphi, \tag{2.39}$$

in which the configuration of ψ^I has already solved two KG equations. The Maxwell equations still give Eq. (2.14), while the Einstein equation reduces to

$$-f - r\frac{df}{dr} - \Lambda r^2 - G_N\left(\frac{d\phi}{dr}\right)^2 = \frac{e^{-\lambda}}{2\rho}\left(\frac{d\lambda}{d\rho} + \rho\left(16\pi G_N\alpha^2 + \frac{d^2\lambda}{d\rho^2}\right)\right), \tag{2.40}$$

$$\frac{1}{2}\frac{d^2 f}{dr^2} + \frac{1}{r}\frac{df}{dr} + \Lambda = G_N\left(\frac{d\phi}{dr}\right)^2. \tag{2.41}$$

Thus, the same $f(r)$ and $\phi(r)$ with Eq. (2.21) solve Eqs. (2.14) and (2.41), and imply the lhs of Eq. (2.40) becomes a constant $-c$. Hence, the rhs of Eq. (2.40) leads to

$$\frac{d\lambda}{d\rho} + \rho\left(16\pi G_N\alpha^2 + \frac{d^2\lambda}{d\rho^2}\right) = -2c\rho e^{\lambda}, \tag{2.42}$$

which is a nonlinear differential equation for $\lambda(\rho)$ if $c \neq 0$. It is hard to find an exact general solution. However, in the case of $c = 0$, Eq. (2.42) reduces to a linear equation that can be exactly solved. The solution is

$$\lambda(\rho) = -4\pi G_N\alpha^2\rho^2 + n\log(\beta\rho). \tag{2.43}$$

Therefore, the full solution for $c = 0$ is given by

$$ds^2 = -\left(-\frac{8\pi G_N M}{\Omega r} + \left(\frac{4\pi}{\Omega}\right)^2\frac{G_N Q^2}{r^2} - \frac{\Lambda r^2}{3}\right)dt^2 + \left(-\frac{8\pi G_N M}{\Omega r} + \left(\frac{4\pi}{\Omega}\right)^2\frac{G_N Q^2}{r^2} - \frac{\Lambda r^2}{3}\right)^{-1}dr^2 + r^2(\beta\rho)^n e^{-4\pi G_N\alpha^2\rho^2}(d\rho^2 + \rho^2 d\varphi^2),$$
$$A_\mu dx^\mu = -\frac{4\pi Q}{\Omega r}dt,$$
$$\psi^1 = \alpha\rho\cos\varphi, \qquad \psi^2 = \alpha\rho\sin\varphi. \tag{2.44}$$

1. *Compare with the planar axionic RN-AdS black hole*

On the other hand, simply demanding λ as a constant also solves Eq. (2.42). Then the constant c should be

$$c = -8\pi G_N\alpha^2 e^{-\lambda}. \tag{2.45}$$

We rescale α and introduce a coordinate transformation

$$\tilde{\alpha} = \alpha e^{-\lambda/2},$$
$$x = e^{\lambda/2}\rho\cos\varphi, \qquad y = e^{\lambda/2}\rho\sin\varphi, \tag{2.46}$$

such that the solution is given by

$$ds^2 = -f(r)dt^2 + \frac{dr^2}{f(r)} + r^2(dx^2 + dy^2),$$
$$f(r) = -8\pi G_N\tilde{\alpha}^2 - \frac{8\pi G_N M}{\Omega r} + \left(\frac{4\pi}{\Omega}\right)^2\frac{G_N Q^2}{r^2} - \frac{\Lambda r^2}{3},$$
$$A_\mu dx^\mu = -\frac{4\pi Q}{\Omega r}dt, \qquad \psi^1 = \tilde{\alpha}x, \qquad \psi^2 = \tilde{\alpha}y, \tag{2.47}$$

which the metric has a planar transverse space $dx^2 + dy^2$. It is worth noting that the planar D-dimensional AdS black hole in Ref. [31] reduces to Eq. (2.47) if $D = 4$ and $\Lambda < 0$. The remarkable feature of such kind of planar black hole achieves momentum relaxation through the configuration of scalars to break the transition symmetries called the holographic axion model [31,32,38]. In the holographic context, it would be convenient to redefine parameters M/Ω, Q/Ω, and Λ to explicitize the horizon location r_H. First, we rewrite Λ as $\Lambda = -3/L^2$ and then adjust the gauge condition for A_μ to make

$$\phi = -\mu\left(1 - \frac{r_H}{r}\right), \tag{2.48}$$

which vanishes on the horizon, but has a finite value on the AdS boundary. Hence, we have relation

$$\mu r_H = 4\pi Q/\Omega. \tag{2.49}$$

Moreover, investigations of holographic models usually apply the coordinate $u = L/r$ such that the flat boundary is at $u = 0$, but we still use the coordinate r in this paper since using r is beneficial to formulate the unified first law, discussed in the next section. Therefore, $r = \infty$ is the AdS boundary. As for M/Ω, the requirement $f(r_H)$ gives

$$M/\Omega = -\alpha r_H^2 + \frac{\mu^2 r_H}{8\pi} + \frac{r_H^3}{8\pi G_N L^2}, \tag{2.50}$$

in which we omit the tilde sign of α. Therefore, the solution (2.47) is reformulated as

$$\begin{aligned} ds^2 &= -f(r)dt^2 + \frac{dr^2}{f(r)} + r^2\delta_{ij}dx^i dx^j, \\ f(r) &= -8\pi G_N\alpha^2 - \frac{r_H}{r}\left(-8\pi G_N\alpha^2 + G_N\mu^2 + \frac{r_H^2}{L^2}\right) \\ &\quad + \frac{G_N\mu^2 r_H^2}{r^2} + \frac{r^2}{L^2}, \\ A_\mu dx^\mu &= \mu\left(1 - \frac{r_H}{r}\right)dt, \qquad \psi^I = \alpha\delta_i^I x^i. \end{aligned} \tag{2.51}$$

Following the method summarized in Ref. [38], we consider the following perturbation around the solution (2.51) to calculate the dc conductivity:

$$\begin{aligned} \delta g_{tx} &= r^2 H_{tx}(r), \qquad \delta g_{rx} = r^2 H_{rx}(r), \\ \delta A_x &= -tE + a(r). \end{aligned} \tag{2.52}$$

No ζ and $\delta\psi^I$ are considered here because we only focus on the electric dc conductivity in this paper; we leave the thermoconductivity for future works. The perturbative Maxwell equation leads to a conserved current

$$\mathcal{J} = -f(r)\delta A_x'(r) + \phi'(r)r^2 H_{tx}(r), \tag{2.53}$$

where $'$ is d/dr for short. We have considered that

$$\frac{d}{dr} = -\frac{u^2}{L}\frac{d}{du} \tag{2.54}$$

will introduce a "−" sign for Eq. (2.53), different from Ref. [38]. In addition, the rx component of the linearized Einstein equation implies a constraint for $H_{rx}(r)$, such that

$$H_{rx}(r) = E\frac{r_H\mu}{4\pi\alpha^2 r^2 f}. \tag{2.55}$$

Then one can obtain the boundary dc conductivity by the horizon data because values of $\mathcal{J}$ are independent of the location r. According to Ref. [38], the perturbation should satisfy the boundary condition near the horizon,

$$\delta A_x' \sim -\frac{E}{f}, \qquad H_{tx}(r) \sim fH_{rx}(r), \tag{2.56}$$

Hence, we obtain

$$\mathcal{J} = \left(1 + \frac{\mu^2}{4\pi\alpha^2}\right)E. \tag{2.57}$$

The 4π factor different from Ref. [38] is due to the unit selection for the Maxwell field. We use $-F^2/(16\pi)$ rather than $-F^2/(4\pi)$ as its Lagrangian in the action (2.1). Notice that Ohm's law is

$$\mathcal{J} = \sigma_{\mathrm{dc}}E. \tag{2.58}$$

We obtain the finite dc conductivity,

$$\sigma_{\mathrm{dc}} = 1 + \frac{\mu^2}{4\pi\alpha^2}. \tag{2.59}$$

It is worth noting that the metric (2.47) has the same t-r part with the hyperbolic RN-AdS black hole, though the transverse space describes a plane. Such an observation is also one motivation in Ref. [83] to construct a hyperbolic black hole in an Einstein-Maxwell-dilation theory shares the same t-r geometry with a planar black hole containing axionic charges. Here, solution II given by Eq. (2.44) hints at a continuing family of transverse shapes between the hyperbolic solution without axions and the planar solution with axions.

We will further calculate the dc conductivity for a general metric describing a deformed topological black hole to end the comparison. We replace the $-8\pi G_N\alpha^2$ and δ_{ij} in Eq. (2.51) to c and $e^{\lambda(x)}\delta_{ij}$ in which the function $\lambda(x)$ satisfies

$$\partial^2\lambda + 16\pi G_N\alpha^2 = -2ce^\lambda, \tag{2.60}$$

where $\partial^2\lambda$ is $\delta^{ij}(\partial^2\lambda/\partial x^i\partial x^j)$ for short. Hence, the following metric, gauge field, and axions also solve the equations of motion:

$$\begin{aligned} ds^2 &= -f(r)dt^2 + \frac{dr^2}{f(r)} + r^2 e^{\lambda(x)}\delta_{ij}dx^i dx^j, \\ f(r) &= c - \frac{r_H}{r}\left(c + G_N\mu^2 + \frac{r_H^2}{L^2}\right) + \frac{G_N\mu^2 r_H^2}{r^2} + \frac{r^2}{L^2}, \\ A_\mu dx^\mu &= \mu\left(1 - \frac{r_H}{r}\right)dt, \qquad \psi^I = \alpha\delta_i^I x^i. \end{aligned} \tag{2.61}$$

Then consider the perturbation

$$\begin{aligned} \delta g_{ti} &= (r^2 H_t(r))\partial_i X, \\ \delta g_{rx} &= (r^2 H_r(r))\partial_i X, \\ \delta A_i &= (-Et + a(r))\partial_i X. \end{aligned} \tag{2.62}$$

Requiring X be a harmonic scalar on $\hat{\mathcal{M}}_2$, i.e., $\partial^2 X = 0$, will solve most equations of motion, but leaves three independent equations that are similar to the simplest holographic axion model discussed above. Those equations ensure the validity of the current (2.53) and the constraint (2.55) by simply replacing α^2 by $-c/(8\pi G_N)$. Hence, they lead to the explicit result of the dc conductivity,

$$\sigma_{\rm dc} = 1 - \frac{2G_N\mu^2}{c}. \tag{2.63}$$

2. Shapes of horizons

We will then study the horizon shapes of solution II. Even if we omit cases of $c \neq 0$ and only focus on cases of $c = 0$ in this article, there are various shapes of the transverse space $\hat{\mathcal{M}}_2$. Again, one can introduce a suitable rescaling to reduce the parameters in the line element (2.44). Hence, the $\hat{\mathcal{M}}_2$ part becomes

$$d\hat{s}^2 = \rho^n e^{-\rho^2}(d\rho^2 + \rho^2 d\varphi^2). \tag{2.64}$$

Thus, only the parameter n controls the $\hat{\mathcal{M}}_2$ geometry. The independent Ricci scalar is

$$\hat{R} = 4\frac{e^{\rho^2}}{\rho^n}, \tag{2.65}$$

which obviously blows up at $\rho = 0$ if $n > 0$. When $n = 0$, the point $\rho = 0$ obviously becomes a regular center, but it becomes subtle for cases of $n < 0$. Suppose we start from a finite value ρ and go along a direction with a fixed φ. Such a path is no doubt a spacelike geodesic, and its affine parameter is the proper distant l, which is determined by

$$\frac{dl}{d\rho} = \rho^{n/2}e^{-\rho^2/2}, \tag{2.66}$$

according to Eq. (2.64). When we get close to $\rho = 0$, $dl/d\rho$ behaves as $\rho^{n/2}$. Thus,

$$l \sim \begin{cases} \rho^{n/2+1}, & \text{if } n \neq -2, \\ \log\rho, & \text{if } n = -2. \end{cases} \tag{2.67}$$

Therefore, for cases of $n \leq -2$, l tends to negative infinity as ρ tends to 0 even though $\hat{R}$ keeps finite; if $-2 < n \leq 0$, both l and $\hat{R}$ have finite values. For cases of $n > 0$, the finite limit of l supports that $\rho = 0$ is the intrinsic singularity.

In addition, when ρ tends to infinity, $dl/d\rho$ will rapidly decrease due to the exponential factor $e^{-\rho^2/2}$. Thus, l will converge to a finite limit, but $\hat{R}$ will blow up within such a finite affine parameter because of Eq. (2.65). Therefore, $\rho = \infty$ is the intrinsic singularity despite the value of n.

We will draw the embedding diagram for typical cases to visualize the above features. Hence, we should define

$$\tilde{r} = \rho^{1+n/2}e^{-\rho^2/2} \tag{2.68}$$

and rewrite Eq. (2.64) as

$$d\hat{s}^2 = -\rho^n e^{-\rho^2}\left(\rho^2 - \frac{n}{2}\right)\left(\rho^2 - \frac{n+4}{2}\right)d\rho^2 + d\tilde{r}^2 + \tilde{r}^2 d\varphi^2, \tag{2.69}$$

in which the sign of the factor $(\rho^2 - n/2)(\rho^2 - (n+4)/2)$ determines the signature of the higher-dimensional flat space. For the region of ρ between values $\sqrt{n/2}$ and $\sqrt{(n+4)/2}$, we introduce

$$\frac{dz_{\rm E}}{d\rho} = \rho^{n/2}e^{-\rho^2/2}\sqrt{-\left(\rho^2 - \frac{n}{2}\right)\left(\rho^2 - \frac{n+4}{2}\right)}, \tag{2.70}$$

which specifies the embedding into an Euclidean space, whereas the Minkowski regions should be ρ smaller than $\sqrt{n/2}$ or larger than $\sqrt{(n+4)/2}$. They lead to the following embedding:

$$\frac{dz_{\rm M}}{d\rho} = \rho^{n/2}e^{-\rho^2/2}\sqrt{\left(\rho^2 - \frac{n}{2}\right)\left(\rho^2 - \frac{n+4}{2}\right)}. \tag{2.71}$$

We will then pick up some typical values of n to draw the embedded diagram.

Figure 14 shows the case of $n = 2$, which is typical for $n > 0$. Figures from left to right represent (1) the $0 < \rho < 1$ region embedded into a Minkowski space; (2) the $1 < \rho < \sqrt{3}$ region embedded into an Euclidean space; (3) the $\rho > \sqrt{3}$ region embedded into a Minkowski space; (4) the full embedding diagram of $\hat{\mathcal{M}}_2$. Points for divergent $\hat{R}$, $\rho = 0$ and $\rho = \infty$, appear in two Minkowski regions. While the geometry of the Euclidean part is smooth.

The case of $n = 0$ is shown in Fig. 15. The left figure represents the $0 \leq \rho < \sqrt{2}$ region embedded into Euclidean space, while the middle one is for the $\rho > \sqrt{2}$ Minkowski region. The right figure is for the whole $\hat{\mathcal{M}}_2$. The regular center $\rho = 0$ is in the Euclidean region, and the singular $\rho = \infty$ is in the Minkowski region.

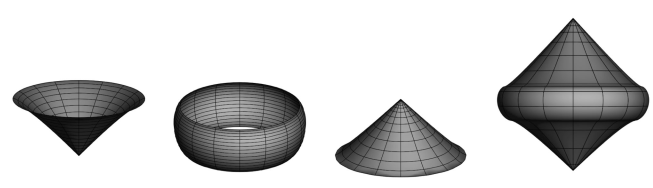

FIG. 14. Embedding diagrams for $n = 2$: from left to right, they are (1) $0 < \rho < 1$, the Minkowski region; (2) $1 < \rho < \sqrt{3}$, the Euclidean region; (3) $\rho > \sqrt{3}$, the Minkowski region; (4) the whole embedding diagram.

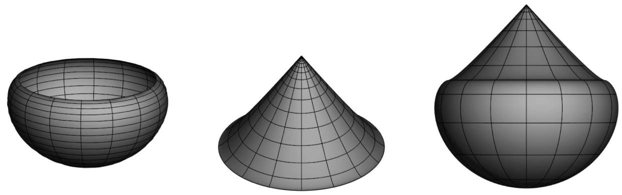

FIG. 15. Embedding diagrams for $n = 0$: the left figure is for the Euclidean region $0 \leq \rho < \sqrt{2}$ containing the regular center $\rho = 0$; the middle figure shows the $\rho > \sqrt{2}$ region embedded into a Minkowski space in which the $\rho = \infty$ is a singular direction. The right one is the whole embedding diagram.

The case of $n = -2$ also contains one Euclidean region and one Minkowski region, as shown in Fig. 16. The left and middle figures are for the $0 \leq \rho < 1$ Euclidean region and the $\rho > 1$ region, respectively. The whole embedding diagram is the right figure. The infinity ρ also appears in the Minkowski region, but the region near $\rho = 0$ is enlarged as a lone tube in the Euclidean region, distinguished with the $n = 0$ case.

A heavier enlargement happens when $n < -2$. Figure 17 includes the cases for $n = -4$ and $n = -6$, entirely embedded into a Minkowski space. They contain $\rho = \infty$ as the center peaks, and the $\rho \sim 0$ regions extended to extreme far-away proper distance.

Solutions I and II show how suitable profiles for axions deform transverse spaces even in $D = 4$. The nontrivial shape makes the physical meaning of parameters M and Q hard to understand. Consider turning off the cosmological constant Λ. Both solutions are not asymptotically flat since the nontrivial shape extends to infinity. Taking $\Lambda \neq 0$ does not make it better. Lacking a well-defined asymptotically structure like Minkowski or AdS indicates the conceptual difficulties for formulating the black hole thermodynamics via the global parameters M and Q. To overcome such a difficulty, we will develop a quasilocal viewpoint based on the MS mass and the unified first law in the next section.

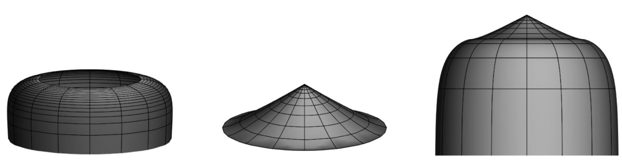

FIG. 16. Embedding diagrams for the $n = -2$ case: the left figure is for $0 \leq \rho < 1$ (Euclidean); the middle one is for $\rho > 1$ (Minkowski); the right figure is the whole embedding diagram.

FIG. 17. The left embedding diagram is for $n = -4$, while the right one is for $n = -6$. There is no Euclidean region in these cases.

III. THE GENERALIZED UNIFIED FIRST LAW

This section will briefly introduce the MS mass and the unified first law and then discuss the thermodynamic method for generating solutions based on them. The method was originally proposed in Ref. [69] for spherically symmetric spacetime. We aim to modify this method to adapt other shapes with nonconstant $\hat{R}(x)$ instead of a sphere. The modified thermodynamic method justifies some *Ansätze* in Eqs. (2.8) and (2.39). Another goal of this section is to show how the unified first law offers a quasilocal viewpoint for black hole thermodynamics.

A. Derived from Einstein equation

This subsection will rederive the unified first law from the Einstein equation. To keep generality, we consider a D-dimensional warped product spacetime $\bar{\mathcal{M}}_{(2)} \times \hat{\mathcal{M}}_{(D-2)}$. Its line element is

$$\begin{aligned} ds^2 &= g_{\mu\nu}(X) dX^\mu dX^\nu \\ &= I_{ab}(u) du^a du^b + r^2(u) \hat{g}_{ij}(x) dx^i dx^j. \end{aligned} \tag{3.1}$$

Coordinate frame $\{X^\mu\}$ of the whole spacetime is specified as $\{u^a, x^i\}$. It is beneficial to choose the following viewpoint. Coordinates u^a label the point in the two-dimensional manifold $\bar{\mathcal{M}}_{(2)}$, while x^i labels the point in the $(D-2)$-dimensional manifold $\hat{\mathcal{M}}_{(D-2)}$. Both manifolds have independent metrics $I_{ab}(u)$ and $\hat{g}_{ij}(x)$. The areal radius $r(u)$ is a scalar function in spacetime, as well as a function in $\bar{\mathcal{M}}_{(2)}$. Its value means enlarging the unit $\hat{\mathcal{M}}_{(D-2)}$ in r times. It is worth emphasizing again that the manifold $\hat{\mathcal{M}}_{(D-2)}$ is not limited to the maximally symmetric space investigated in Refs. [66,70]. We do not presume a constant Ricci scalar $\hat{R}(x)$ of $\hat{\mathcal{M}}_{(D-2)}$. Meanwhile, we assume that the manifold $\hat{\mathcal{M}}_{(D-2)}$ has a finite $(D-2)$-dimensional "unit area" Ω, or just the finite part of the $\hat{\mathcal{M}}_{(D-2)}$ with the volume unit area is concerned.

We then decompose the Einstein equation by applying results in Appendix A. Results of ab components are

$$\begin{aligned} &-\frac{D-2}{r}\left(\bar{\nabla}_a \bar{\nabla}_b r - \frac{1}{2} I_{ab} \bar{\nabla}^2 r\right) \\ &\quad + \frac{D-2}{2r} I_{ab}\left(\bar{\nabla}^2 r - \frac{D-3}{r}(\mathcal{K} - I^{rr})\right) + \Lambda I_{ab} \\ &= 8\pi G_N T_{ab}, \end{aligned} \tag{3.2}$$

while ij components are

$$\hat{R}_{ij} - (D-3)\mathcal{K}\hat{g}_{ij} - \hat{g}_{ij}\left(\frac{r^2}{2}\bar{R} - (D-3)r\bar{\nabla}^2 r + \frac{(D-3)(D-4)}{2}(\mathcal{K} - I^{rr}) - \Lambda r^2\right) = 8\pi G_N T_{ij}, \tag{3.3}$$

where I^{rr} is $\bar{\nabla}_a r \bar{\nabla}^a r$ for short, $\bar{\nabla}$ and $\widehat{\nabla}$ are the Levi-Civita connection of $\bar{\mathcal{M}}_{(2)}$ and $\hat{\mathcal{M}}_{(D-2)}$, respectively, and $\mathcal{K}$ is the reduced Ricci scalar of $\hat{\mathcal{M}}_{(D-2)}$ given by

$$\mathcal{K} = \frac{\hat{R}}{(D-2)(D-3)}. \tag{3.4}$$

The so-called unified first law is directly derived from Eq. (3.2) and hints at suitable definitions for the MS mass. To show this, we need to define the energy supply vector Ψ^a and the work term W first. Namely,

$$\Psi^a = \left(T^{ab} - \frac{1}{2}T_{cd}I^{cd}I^{ab}\right)\bar{\nabla}_b r,$$
$$W = -\frac{1}{2}T_{ab}I^{ab}. \tag{3.5}$$

It is worth noting that the energy supply vector is constructed by projecting the traceless tensor

$$\tilde{T}^{ab}_{\text{traceless}} = T^{ab} - \frac{1}{2}T_{cd}I^{cd}I^{ab}, \tag{3.6}$$

on the direction $\bar{\nabla}^a r$. With the Einstein equation (3.2), Ψ^a and W should satisfy

$$\frac{D-2}{2r}((\bar{\nabla}^2 r)\bar{\nabla}_a r - \bar{\nabla}_a I^{rr}) = 8\pi G_N \Psi_a, \tag{3.7}$$

$$\frac{D-2}{2r}\left(\frac{D-3}{r}(\mathcal{K} - I^{rr}) - \bar{\nabla}^2 r\right) - \Lambda = 8\pi G_N W, \tag{3.8}$$

where we have lowered the index of the energy supply vector Ψ^a. Obviously, the term with $\bar{\nabla}^2 r$ factor would disappear in the combination $\Psi_a + W\bar{\nabla}_a r$ due to the common factor $(D-2)/(2r)$ in Eqs. (3.7) and (3.8). Moreover, even considering the situation of nonconstant $\mathcal{K}$, it should only depend on x, i.e.,

$$\bar{\nabla}_a \mathcal{K} = \frac{\partial \mathcal{K}}{\partial u^a} = 0. \tag{3.9}$$

Therefore, we have

$$-\bar{\nabla}_a I^{rr} = \bar{\nabla}_a(\mathcal{K} - I^{rr}), \tag{3.10}$$

such that

$$\frac{D-2}{2r}\left(\bar{\nabla}_a(\mathcal{K} - I^{rr}) + \frac{D-3}{r}(\mathcal{K} - I^{rr})\bar{\nabla}_a r\right) - \Lambda\bar{\nabla}_a r = 8\pi G_N(\Psi_a + W\bar{\nabla}_a r). \tag{3.11}$$

The lhs of (3.11) further hints at the following simplification:

$$\bar{\nabla}_a\left(\frac{D-2}{16\pi G_N}r^{D-3}(\mathcal{K} - I^{rr}) - \frac{\Lambda}{8\pi G_N}\frac{r^{D-1}}{D-1}\right) = r^{D-2}(\Psi_a + W\bar{\nabla}_a r), \tag{3.12}$$

which indicates that $r^{D-2}(\Psi_a + W\bar{\nabla}_a r)$ equals a total derivative of some scalar function on $\bar{\mathcal{M}}_{(2)}$. Multiply the size Ω of the unit $\hat{\mathcal{M}}_{(D-2)}$. The lhs of Eq. (3.12) hints at

$$M_{\text{MS}}(u,x) = \frac{(D-2)\Omega}{16\pi G_N}r^{D-3}(\mathcal{K}(x) - I^{rr}) - \frac{\Lambda}{8\pi G_N}\frac{\Omega r^{D-1}}{D-1}, \tag{3.13}$$

which defines the MS mass with x dependence. Introduce area and "volume,"

$$A = \Omega r^{D-2}, \qquad V = \Omega\frac{r^{D-1}}{D-1}, \tag{3.14}$$

for Eq. (3.12), such that

$$\bar{\nabla}_a M_{\text{MS}} = A\Psi_a + W\bar{\nabla}_a V, \tag{3.15}$$

which serves as the unified first law with x dependence.

An alternative expression for the MS mass and the unified first law is integrating out x to define the average MS mass, concretely,

$$m_{\text{MS}}(u) = \frac{(D-2)\Omega}{16\pi G_N}r^{D-3}(k - I^{rr}) - \frac{\Lambda}{8\pi G_N}\frac{\Omega r^{D-1}}{D-1}, \tag{3.16}$$

in which k is the average $\mathcal{K}$ in the sense of

$$k = \Omega^{-1}\int_{\hat{\mathcal{M}}_{(D-2)}}\mathcal{K}(x)\sqrt{\hat{g}(x)}d^{D-2}x, \tag{3.17}$$

and define the average work term

$$w(u) = \Omega^{-1}\int_{\hat{\mathcal{M}}_{(D-2)}}W(u,x)\sqrt{\hat{g}(x)}d^{D-2}x. \tag{3.18}$$

On the other hand, the energy supply vector in general relativity does not depend on x according to Eq. (3.7). There is no need to define the average energy supply vector ψ^a since ψ^a should be the same as Ψ^a. Therefore, the unified first law has the following average version:

$$\bar{\nabla}_a m_{\text{MS}} = A\psi_a + w\bar{\nabla}_a V. \tag{3.19}$$

We conclude that two versions of the unified first law are needed to include shapes for $\hat{\mathcal{M}}_{(D-2)}$ with a nonconstant Ricci scalar. The nonaverage first law (3.15) and the average one (3.19) share the same $A\psi$ term. It would be interesting to compare the holographic viewpoint. If we treat $\hat{\mathcal{M}}_{(D-2)}$ with fixed r as the holographic screen with a fixed r, which is similar to the screen defined in Refs. [41,42], then it is natural to view $M_{\rm MS}/\Omega$, A/Ω, and V/Ω as some screen densities, but the $A\psi_a$ term in Eq. (3.15) will be replaced by the $r^{D-2}\psi_a$ term.

B. Thermodynamics method

If all matter sources contribute an energy-momentum tensor satisfying the following two conditions: (i) the sum of energy supply vectors vanishes

$$\sum_{(i)}\psi^a_{(i)} = 0; \tag{3.20}$$

(ii) the sum of average work terms

$$w_{\rm tot} \equiv \sum_{(i)} w_{(i)} = 0, \tag{3.21}$$

only depends on r except the situation of

$$w_{\rm tot} = \frac{(D-2)(D-3)k}{16\pi G_N r^2} - \frac{\Lambda}{8\pi G_N}, \tag{3.22}$$

where (i) labels the composition of those sources, then the line element $d\bar{s}^2$ is determined as

$$d\bar{s}^2 = -I^{rr}dt^2 + \frac{dr^2}{I^{rr}}, \tag{3.23}$$

where the function I^{rr} should be

$$I^{rr} = k - \frac{16\pi G_N}{(D-2)r^{D-3}}\left(M/\Omega + \int^r w_{\rm tot}(\xi)\xi^{D-2}d\xi\right) - \frac{2\Lambda r^2}{(D-1)(D-2)}. \tag{3.24}$$

It is straightforward to obtain Eq. (3.24) via the average unified first law as the first step. The average unified first law under conditions (i) and (ii) gives

$$\bar{\nabla}_a m_{\rm MS} = w_{\rm tot}(r)\Omega r^{D-2}\bar{\nabla}_a r. \tag{3.25}$$

Since the sum of average work terms serves as a function of r, directly integrating r implies

$$m_{\rm MS}(r) = M + \Omega\int^r w_{\rm tot}(\xi)\xi^{D-2}d\xi, \tag{3.26}$$

where M is the mass parameter that can absorb the integral constant from the second term. Therefore, Eq. (3.16) implies that I^{rr} should be Eq. (3.24).

The next task is to confirm Eq. (3.23). A concrete calculation under the Eddington-Finkelstein-like coordinates makes it explicit. Appendix B gives some useful results. First, the line element $I_{ab}du^a du^b$ can be generally written as

$$d\bar{s}^2 = -\frac{f(v,r)}{\sigma^2(v,r)}dv^2 + \frac{2dvdr}{\sigma(v,r)}, \tag{3.27}$$

where the function $f(v,r)$ is exactly I^{rr}. Such coordinate frame can be always chosen on $\bar{\mathcal{M}}_{(2)}$, thus respecting the generality. In addition, the Laplacian of r on $\bar{\mathcal{M}}_{(2)}$ is

$$\bar{\nabla}^2 r = f' - f\frac{\sigma'}{\sigma}. \tag{3.28}$$

Thus, Eq. (3.7) forces the total energy supply vector to become

$$\Psi_a = -\frac{D-2}{16\pi G_N}\frac{f}{r}\frac{\sigma'}{\sigma}\bar{\nabla}_a r. \tag{3.29}$$

Obviously, $\Psi_a = 0$ if $\sigma' = 0$. In this case, σ is at least a nonvanishing function of v. Appendix B also explains why we should have $\sigma \neq 0$. Despite the concrete expression, the coordinate transformation

$$t \equiv \int^v \frac{d\eta}{\sigma(\eta)} + \int^r \frac{d\xi}{f(\xi)} \tag{3.30}$$

changes Eq. (3.27) as Eq. (3.23). Hence, the proof is almost completed. On the other hand, it is worth noting that the case of $I^{rr} = 0$ may ruin such a proof. Fortunately, the condition $I^{rr} = 0$ is too strong such that the average MS mass is fixed as

$$m_{\rm MS} = \frac{(D-2)\Omega}{16\pi G_N}kr^{D-3} - \frac{\Lambda\Omega r^{D-1}}{8(D-1)\pi G_N}. \tag{3.31}$$

Therefore, the work term becomes Eq. (3.22), which we have excluded in condition (ii).

This method simplifies solving the ab components of the Einstein equation. Hence, it simplifies the proof of Birkhoff's theorem. A spherically symmetric $D = 4$ spacetime is a warped product $\bar{\mathcal{M}}_{(2)} \times S^2$ because the spherical symmetry indicates the spacetime can be foliated by a set of orbits of the $SO(3)$ rotation group, i.e., a set of spheres (see Ref. [84]). Thus, the metric should be Eq. (3.1), while the $\hat{g}_{ij}$ serves as the metric of a unit sphere with $k = 1$. The vacuum condition implies $\psi_a = 0$ and $W = 0$ hence the MS mass is a constant M. Therefore, the above proof forces the line element $d\bar{s}^2$ to become Eq. (3.23), where the function I^{rr} is $1 - 2G_N M/r$. Combining with the line element of a unit sphere $d\Omega^2$, the whole metric for the solution is

$$ds^2 = -\left(1 - \frac{2G_N M}{r}\right)dt^2 + \frac{dr^2}{1 - \frac{2G_N M}{r}} + r^2 d\Omega^2, \qquad (3.32)$$

namely, the Schwarzchild metric. Finally, we should substitute this result to the constraint equations (3.3) to ensure it is satisfied. Such a proof for Birkhoff's theorem can be easily generalized to higher dimensions and the situation with a cosmological constant. Moreover, this method hints at a simplified construction and probably a higher-dimensional generalization for our solutions. We will then check the Maxwell equation for gauge field A_μ and KG equations for axions ψ^I, and find out their energy supply vectors and work terms.

1. Maxwell field

A simple *Ansatz* for the gauge 1-form,

$$A = -\phi(v, r)dv, \qquad (3.33)$$

will solve the Maxwell equation without knowing details about the metric. This *Ansatz* implies the strength 2-form $F = dA$ should be

$$F = -\phi' dr \wedge dv. \qquad (3.34)$$

Then, read nonvanishing components

$$F_{rv} = -F_{vr} = -\phi'. \qquad (3.35)$$

Notice that

$$F^{vr} = I^{vr} I^{rv} F_{rv}, \qquad (3.36)$$

the Maxwell equations imply

$$\frac{\partial}{\partial v}(r^{D-2}\sigma\phi') = \frac{\partial}{\partial r}(r^{D-2}\sigma\phi') = 0, \qquad (3.37)$$

such that the electric field strength

$$-\phi' = \frac{4\pi Q/\Omega}{\sigma r^{D-2}} \qquad (3.38)$$

is obtained without knowing the concrete expression of functions f and σ in the metric. On the other hand, the energy-momentum tensor for the Maxwell field in D dimensions is the same with Eq. (2.5). We thus calculate its nonvanishing components as

$$T_{vv} = 2\pi\left(\frac{Q/\Omega}{r^{D-2}}\right)^2 \frac{f}{\sigma^2},$$
$$T_{vr} = T_{rv} = -2\pi\left(\frac{Q/\Omega}{r^{D-2}}\right)^2 \frac{1}{\sigma},$$
$$T_{ij} = 2\pi \frac{(Q/\Omega)^2}{r^{2(D-3)}} \hat{g}_{ij}. \qquad (3.39)$$

Then the work term for the electromagnetic field is

$$W_{\mathrm{em}} = 2\pi \frac{(Q/\Omega)^2}{r^{2(D-2)}}, \qquad (3.40)$$

while its energy supply vector vanishes, namely, $\Psi^a_{\mathrm{em}} = 0$. Since W_{em} does not rely x, the averaged work term w_{em} is the same.

2. Linear axions

Consider *Ansatz*

$$\psi^I = \alpha \delta^I_i x^i. \qquad (3.41)$$

Scalars satisfy Eq. (2.4) if coordinates x^i are harmonic. To simply their energy-momentum tensor, define

$$\Phi_{ij} = \delta_{IJ} \frac{\partial\psi^I}{\partial x^i} \frac{\partial\psi^J}{\partial x^j} \qquad (3.42)$$

and label $\Phi(x)$ as the trace of Φ_{ij}, namely,

$$\Phi(x) \equiv \hat{g}^{ij}(x)\Phi_{ij}. \qquad (3.43)$$

We keep the expression $\Phi(x)$ and $\hat{g}^{ij}(x)$ to remind us that they may depend on x. Hence, the axions contain the following energy-momentum tensor:

$$T_{ab} = -\frac{\Phi(x)}{2r^2} I_{ab}, \qquad T_{ij} = \Phi_{ij} - \frac{\Phi(x)}{2}\hat{g}_{ij}(x), \qquad (3.44)$$

in which T_{ab} components only contain trace parts. Thus, it also has a vanishing energy supply vector $\Psi^a_{\mathrm{axions}} = 0$, while its work term is

$$W_{\mathrm{axions}} = \frac{\Phi(x)}{2r^2}, \qquad (3.45)$$

which may depend on x. Simply integrate out x, then we obtain the averaged work term

$$w_{\mathrm{axions}} = \frac{\phi_{\mathrm{ax}}}{2r^2}, \qquad (3.46)$$

in which

$$\phi_{\mathrm{ax}} \equiv \Omega^{-1} \int \Phi(x)\sqrt{\hat{g}} d^{D-2}x. \qquad (3.47)$$

3. Guide for Ansätze and generalization

The above thermodynamics method is valid since the electric field and those axion profiles lead to a vanishing total energy supply vector. Summing up all work terms as functions of r, Eqs. (3.40) and (3.46) will contribute

$$\begin{aligned} I^{rr} &= k - \frac{16\pi G_N}{(D-2)r^{D-3}}\left(M/\Omega - \frac{1}{D-3}\frac{(4\pi Q/\Omega)^2}{2r^{D-3}} + \frac{\phi_{\rm ax}}{2(D-3)}r^{D-3}\right) - \frac{2\Lambda r^2}{(D-1)(D-2)} \\ &= c - \frac{16\pi G_N}{(D-2)}\frac{M/\Omega}{r^{D-3}} + \frac{2G_N}{(D-2)(D-3)}\frac{(4\pi Q/\Omega)^2}{r^{2(D-3)}} - \frac{2\Lambda r^2}{(D-1)(D-2)}, \end{aligned} \tag{3.48}$$

where

$$c = k - \frac{8\pi G_N}{(D-2)(D-3)}\phi_{\rm ax}. \tag{3.49}$$

It is worth noting that the x-dependent unified first law gives

$$c = \mathcal{K}(x) - \frac{8\pi G_N \Phi(x)}{(D-2)(D-3)}, \tag{3.50}$$

which indicates that, even though $\mathcal{K}$ and Φ may depend on x, c is a constant. Then we will check the constraint equation (3.3) which leads to

$$\begin{aligned} &\hat{R}_{ij} - \frac{(D-2)(D-3)}{2}\mathcal{K}\hat{g}_{ij} + (D-3)(D-4)\frac{c}{2}\hat{g}_{ij} \\ &\quad = 8\pi G_N\left(\Phi_{ij} - \frac{1}{2}\Phi\hat{g}_{ij}\right). \end{aligned} \tag{3.51}$$

If $D > 4$, the trace of Eq. (3.51) matches Eq. (3.50). Up to here, the Maxwell equation is solved; KG equations are solved by choosing harmonic coordinates, and the thermodynamics method simplifies solving the ab components of the Einstein equation. Thus, Eq. (3.51) is the only equation left to be solved for higher-dimensional generalization of solutions (2.21) and (2.44).

On the other hand, if $D = 4$, there is

$$\hat{R}_{ij} = \mathcal{K}\hat{g}_{ij}, \tag{3.52}$$

because the transverse space is two-dimensional. Moreover, the lhs of Eq. (3.51) is zero since the term with c vanishes in the case of $D = 4$. Therefore,

$$\Phi_{ij} - \frac{\Phi}{2}\hat{g}_{ij} = 0 \tag{3.53}$$

is the constraint condition for axions and the spatial geometry $\hat{g}_{ij}$. A nontrivial geometry with nonconstant $\mathcal{K}$ implies a nonconstant Φ. Hence, the condition (3.53) excludes the possibility of a single axion field. Instead, the geometry with nonconstant $\mathcal{K}$ requires at least two axions, like the theory described by the action (2.1).

The above discussion justifies *Ansätze* (2.8) and (2.39) for specifying a concrete $\hat{g}_{ij}$. Equation (2.8) is inspired by the unified expression

$$d\hat{s}^2 = \frac{d\rho^2}{1-k\rho^2} + \rho^2 d\varphi^2, \tag{3.54}$$

as the line element for sphere $k = 1$, plane $k = 0$, and hyperbolic surface $k = -1$. Equation (2.8) only introduces a deformed term $e(\rho)$ in $\hat{g}_{\rho\rho}$. Though coordinate ρ is not a harmonic function, it can be transformed as $p(\rho)$ such that the line element $\hat{g}_{ij}dx^i dx^j$ becomes

$$d\hat{s}^2 = \rho^2(p)(dp^2 + d\varphi^2), \tag{3.55}$$

in which $\rho(p)$ is the inversed function for $p(\rho)$. Then p is harmonic. Hence, $\psi^1 = \alpha p$ solved the Laplace equation (2.4) for $I = 1$. Finally, Eq. (2.19) is exactly derived from Eq. (3.50).

As for Eq. (2.39), first, any two-dimensional metric with Euclidean signature can be written as

$$d\hat{s}^2 = \exp(\lambda(x,y))(dx^2 + dy^2), \tag{3.56}$$

in which the coordinates $\{x, y\}$ are already harmonics. Then Eq. (3.50) reduces to Eq. (2.60). Furthermore, we turn to the polar coordinate via

$$x = \rho\cos\varphi, \qquad y = \rho\sin\varphi. \tag{3.57}$$

If one poses a rotational symmetry by requiring that $\partial/\partial\varphi$ is a Killing vector field, the constraint equation for the shape of transverse space, Eq. (2.60), further deduces to Eq. (2.42).

C. Black hole thermodynamics

Though the parameter M is exactly the ADM mass in the asymptotic flat case, it seems difficult to be identified as the "mass" for more general situations due to a lack of a suitable asymptotical structure. Nevertheless, the unified first law provides a quasilocal viewpoint without relying on the interpretation of global parameters. Relevant parameters like MS mass, work terms of electric field [Eq. (3.40)], and axions [Eq. (3.46)] are well defined as quasilocal quantities. If we let them take values on the horizon, the unified first law implies the first law of black hole thermodynamics in terms of such quasilocal parameters. For instance, consider a tiny falling energy package that goes through the trapping horizon, which is defined as a hypersurface foliated by marginal surfaces. The horizon

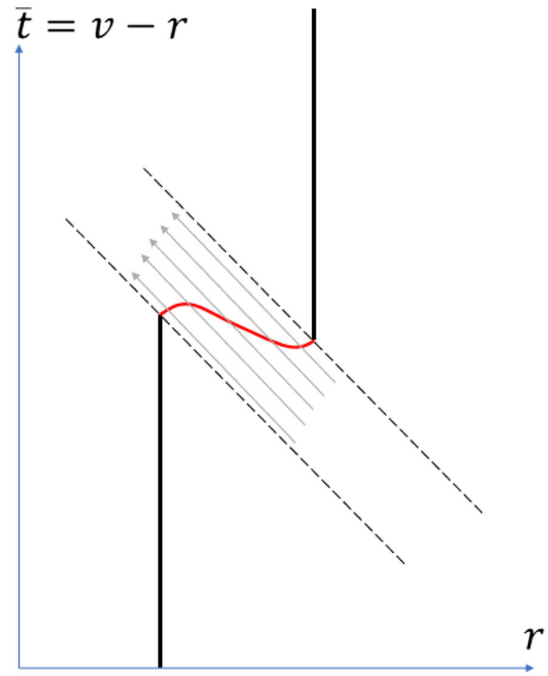

FIG. 18. The time coordinate v is the null retarded time, while $\bar{t}$ is given by $v - r$. Such a sketch describes a falling process changing the size of the trapping horizon. The red curve represents the evolving tapping horizon. Gray arrows portray the in-falling energy package. Both the initial and final moment are marked by gray dotted lines, while Killing horizons are indicated by black lines.

has vanishing expansion. Hence, the equation $I^{rr} = 0$ determines its location (see Appendix B). As shown in Fig. 18, during the accretion, the horizon begins as a Killing horizon and finally settles down as a new Killing horizon. To ensure the unified first law is valid, it is assumed that the $\hat{\mathcal{M}}_{(D-2)}$ part keeps unchanged. The trapping horizon only changes its size during the process. Select a vector z^a tangent to the trapping horizon, i.e.,

$$(z^a \bar{\nabla}_a I^{rr})_H = 0, \tag{3.58}$$

and donate

$$\delta f = (z^a \bar{\nabla}_a f)_H, \tag{3.59}$$

then according to Eq. (3.7), contracting z^a with the $A\psi_a$ generates the $\kappa_{\rm geo}\delta A/(8\pi G_N)$ term, which is the equivalent expression of the heat flow term $T\delta S$. $\kappa_{\rm geo}$ is

$$\kappa_{\rm geo} \equiv \frac{1}{2}\bar{\nabla}^2 r, \tag{3.60}$$

namely, the geometric surface gravity given in [66,85]. The tunneling approach for Hawking radiation in dynamical spacetime confirms the relationship between $\kappa_{\rm geo}$ at the horizon and the horizon temperature [59–63]

$$T = \left(\frac{\kappa_{\rm geo}}{2\pi}\right)_{\rm horizon}. \tag{3.61}$$

Remarkably, two versions of the unified first law, Eqs. (3.15) and (3.19), become

$$\delta M_{\rm MS} - W_H \delta V_H = \delta m_{\rm MS} - w_H \delta V_H = \frac{\kappa_{\rm geo}\delta A}{8\pi G_N}. \tag{3.62}$$

Suppose the difference between the final state and the initial state is tiny enough such that the changes for global parameters are

$$\delta M \simeq M_{\rm fin} - M_{\rm ini}, \qquad \delta Q_{(i)} \simeq Q_{\rm i.fin} - Q_{\rm i.ini} \ldots, \tag{3.63}$$

while W_H, w_H, and $\kappa_{\rm geo}$ are taken as values on the initial Killing horizon, especially $\kappa_{\rm geo} = \kappa_H$ (see Appendix B). They should satisfy

$$\delta M - \sum_i \Phi_{(i).H}\delta Q_{(i)} = \frac{\kappa_H \delta A}{8\pi G_N}, \tag{3.64}$$

where $\Phi_{(i).H}$ should be treated as the thermoconjugate quantity of $Q_{(i)}$. Thus, there is

$$\begin{aligned} \delta M_{\rm MS} - W_H\delta V_H &= \delta m_{\rm MS}(r_H) - w_H \delta V_H \\ &= \delta M - \sum_i \Phi_{(i),H}\delta Q_{(i)}, \end{aligned} \tag{3.65}$$

which connects the quasilocal viewpoint with the global viewpoint (the second line) for the first law. If we apply Eq. (3.65) to our solutions, one obtains

$$\delta M_{\rm MS}(r_H) - W_H \delta V_H = \delta M - \frac{4\pi Q}{\Omega r_H}\delta Q + \frac{\Omega r_H}{2}\delta\Phi, \tag{3.66}$$

in which $\delta\Lambda$ and $\delta\mathcal{K}$ do not enter the global first law deduced from the unified first law shown by the rhs. It seems consistent with the restricted phase space formalism. Despite the global mass parameter M lacking satisfactory definitions at the present stage, the formal expression of the rhs in Eq. (3.66) still makes sense due to the well-defined unified first law. Moreover, both the parameter from the curvature of the transverse space and the axionic parameter join the first law via Eq. (3.50). It indicates that we should consider the axionic charge and the new thermodynamical quantity from the curvature, no matter whether the new quantity is the topological charge, color charge, or center charge. A more serious problem is that metrics in our solutions violate the translational symmetries along transverse directions. Thus, it seems questionable to state "homogeneity" from the first sight. However, the validity of the formal expression requires an appropriate interpretation. We expect the scaling property may be the more suitable starting point. Nevertheless, those solutions sharpen the issue of Euler homogeneity.

Nevertheless, the MS mass hints at the concept of usable energy for a black hole with a positive Ricci scalar, i.e., $\mathcal{K} > 0$. Suppose r_H is the location of the black hole horizon. Since the black hole horizon area does not decrease when suitable energy conditions are not violated, it is reasonable to treat the MS mass on the horizon as the irreducible mass, namely,

$$m_{\mathrm{irr}} \equiv \frac{(D-2)\Omega}{16\pi G_N} \mathcal{K} r_H^{D-3}. \tag{3.67}$$

Then we further define usable energy as

$$m_{\mathrm{usable}}(r) \equiv m_{\mathrm{MS}}(r) - m_{\mathrm{irr}}, \tag{3.68}$$

outside the horizon $r > r_H$. The mass parameter M does not appear in $m_{\mathrm{usable}}(r)$. Instead, the difference of work terms between location r and horizon r_H determines such a new definition. Let r tend to infinity, then one obtains the total usable energy. The concept of usable energy provides an interesting understanding for Ref. [86], which discussed the possibility of a Schwarzchild black hole as a battery. A charging process makes the black hole become an RN black hole. Hence, the rest energy of the in-falling material is transformed into the usable energy of the black hole, while a suitable discharging process will extract such usable energy. Such an argument seems also valid when turning on the axions and cosmological constant.

IV. SUMMARY

In this article, we obtained two novel solutions, Eqs. (2.21) and (2.44), in the simplest holographic axion model, in which the two axions serve as free scalars with canonical kinetic terms. These novel solutions contain transverse spaces with nonconstant Ricci scalars, distinguished from topological RN solutions or planar axionic solutions or solutions with a horizon geometry as an Einstein space [87]. When the cosmological constant is negative, these solutions can describe black holes with deformed horizon shapes. We draw embedding diagrams for various situations. Their shapes usually contain a part embedded into a flat Euclidean space and some parts embedded into a Minkowski space. Solution I allows a regular transverse space, while a singular direction usually appears in other cases, including solution II. We also calculate the dc conductivity for a topological black hole with a generally deformed shape. Compared to the planar axionic AdS black hole, the nonconstant Ricci scalar cancels the direction dependence of the axion configuration. Such a cancellation contributes to the constant that leads to the finite dc conductivity.

In addition, we rederive the unified first law from the Einstein equation in detail. The advantage of applying the unified first law is twofold. First, the unified first law extracts the crucial structure hidden in the Einstein equation. Based on such a structure, we improve the thermodynamics method proposed originally in Ref. [69] to adapt to the situations of deformed transverse spaces. It is an efficient method to construct solutions in which the metric is a warped product. The resulting constraint equations (3.50) and (3.51) hints at how to generalize Eqs. (2.21) and (2.44), i.e., the charged topological black holes with deformed horizon. Second, the unified first law provides a quasilocal viewpoint for the horizon thermodynamics. The MS mass is a mathematically well-defined quasilocal mass. Despite the concrete meaning of the mass parameter M, one can always reinterpret the global first law of black hole thermodynamics as the well-defined unified first law on the horizon. In recent years, several anisotropic black holes with spacetime geometries beyond warped products have been obtained in Gauss-Bonnet gravity [88,89]. Moreover, the improved thermodynamics method requires a vanishing energy supply vector, thus it is less valid for studying black holes with scalar hairs or other cases with hidden scalar degrees of freedom [57,90–92]. We expect the further generalized unified first law adapting situations including new horizon shapes, scalar hairs, and rotation (like Refs. [74,93]) may bring some unexpected insight for a deeper understanding of quasilocal energy [94], the relationship between thermodynamics and gravity [95–99], Kerr/CFT duality [100], and even quantum gravity [82].

Nevertheless, an understanding from the global viewpoint of our novel solutions is still lacking. The direction-dependent Ricci scalar $\hat{R}(x)$ sharpens the issue of introducing new thermodynamical extended quantities to ensure the Euler homogeneity of the first law. To the best of our knowledge, this issue is attached by various approaches, including topological charge [41,42], color charge [49], and center charge [48]. They play a similar role for topological RN black holes as the axionic charge played for planar axionic black holes. Furthermore, our solutions show that effects from the curvature and axions can coexist. It seems a challenge to clarify the interconnection between these charges. We left this issue for future work.

ACKNOWLEDGMENTS

The author thanks Ali Akil, Yusen An, Zhongying Fan, Hyat Huang, Yuxuan Peng, Hongwei Tan, Junlan Xian, Cong Zhang, and the anonymous reviewer for their constructive suggestions. He is also grateful for the support of Mayumi Aoki and Ryoko Nishikawa when the author was at Kanazawa University.

APPENDIX A: CALCULATE $\Gamma^{\lambda}{}_{\mu\nu}$ AND $R^{\lambda}{}_{\rho\mu\nu}$

This appendix shows an efficient method for calculating the Levi-Civita connection and Riemann tensor. Usually, the components of the Levi-Civita connection for a given metric are calculated by

$$\Gamma^{\lambda}_{\mu\nu} = \frac{1}{2} g^{\lambda\sigma}\left(\frac{\partial g_{\mu\sigma}}{\partial x^{\nu}} + \frac{\partial g_{\nu\sigma}}{\partial x^{\mu}} - \frac{\partial g_{\mu\nu}}{\partial x^{\sigma}}\right). \tag{A1}$$

The geodesic equations give hints to finding the trick. Consider the geodesic equations

$$\begin{aligned}\frac{d^2 x^{\lambda}}{d\tau^2} &+ \Gamma^{\lambda}_{\mu\nu}\frac{dx^{\mu}}{d\tau}\frac{dx^{\nu}}{d\tau} \\ &= \frac{d^2 x^{\lambda}}{d\tau^2} + g^{\lambda\sigma}\left(\frac{dg_{\sigma\nu}}{d\tau}\frac{dx^{\nu}}{d\tau} - \frac{1}{2}\frac{\partial g_{\mu\nu}}{\partial x^{\sigma}}\frac{dx^{\mu}}{d\tau}\frac{dx^{\nu}}{d\tau}\right) = 0,\end{aligned} \tag{A2}$$

in which

$$\frac{dg_{\sigma\nu}}{d\tau} = \frac{\partial g_{\sigma\nu}}{\partial x^{\mu}}\frac{dx^{\mu}}{d\tau}. \tag{A3}$$

If the second-order derivative term is ignored, then the structure

$$\Gamma^{\lambda}_{\mu\nu} dx^{\mu} dx^{\nu} = g^{\lambda\sigma}\left(dg_{\sigma\nu}dx^{\nu} - \frac{1}{2}\frac{\partial ds^2}{\partial x^{\sigma}}\right) \tag{A4}$$

is extracted. It serves as a coordinate-dependent rank-two symmetric tensor, in which $\partial ds^2/\partial x^{\sigma}$ is the short notation of $(\partial g_{\mu\nu}/\partial x^{\sigma})dx^{\mu}dx^{\nu}$. Since the coordinate frame is fixed under a particular calculation, one can simply treat $g_{\sigma\nu}$ as several functions of x^{μ} and $dg_{\sigma\nu}$ represents their differential. The trick is to calculate the structure (A4) rather than to calculate components of Eq. (A1) one by one. Now we use this trick to calculate the Levi-Civita connection of the metric (3.1). The components of its inverse metric are

$$g^{ab} = I^{ab}, \qquad g^{ij} = \frac{\hat{g}^{ij}}{r^2}. \tag{A5}$$

Thus, Eq. (A4) gives

$$\begin{aligned}\Gamma^{a}{}_{\mu\nu}dx^{\mu}dx^{\nu} &= \bar{\Gamma}^{a}{}_{bc}du^{b}du^{c} - (r\bar{\nabla}^{a}r)\hat{g}_{ij}dx^{i}dx^{j}, \\ \Gamma^{i}{}_{\mu\nu}dx^{\mu}dx^{\nu} &= 2\frac{\bar{\nabla}_{a}r}{r}du^{a}dx^{i} + \hat{\Gamma}^{i}{}_{jk}dx^{j}dx^{k}.\end{aligned} \tag{A6}$$

Here, the property $\partial r/\partial u^a = \bar{\nabla}_a r$ is used. Noticing that product terms like $du^a dx^i$ are the short notation for symmetric tensor product $(du^a dx^i \otimes dx^i du^a)/2$, every component can be correctly read as

$$\begin{aligned}\Gamma^{a}{}_{bc} &= \bar{\Gamma}^{a}_{bc}, \qquad & \Gamma^{a}{}_{ij} &= -rI^{ab}\frac{\partial r}{\partial u^b}\hat{g}_{ij}, \\ \Gamma^{i}{}_{aj} &= \frac{1}{r}\frac{\partial r}{\partial u^a}\delta^{i}_{j}, \qquad & \Gamma^{i}{}_{jk} &= \hat{\Gamma}^{i}_{jk}.\end{aligned} \tag{A7}$$

It is worth noting that the components Γ^{a}_{bc} and Γ^{i}_{jk} are just the independent Levi-Civita connection of $\bar{\mathcal{M}}_{(2)}$ and $\hat{\mathcal{M}}_{(D-2)}$, respectively. The author would like to introduce the covariant differential operator $\bar{\nabla}_a$ for $\bar{\mathcal{M}}_{(2)}$ and $\hat{\nabla}_i$ for $\hat{\mathcal{M}}_{(D-2)}$. The areal radius $r(u)$ can be treated as a scalar field in $\bar{\mathcal{M}}_{(2)}$. The notation $\bar{\nabla}_a r$ also means $\partial r/\partial u^a$, while $\bar{\nabla}^a r$ means $I^{ab}(\partial r/\partial u^b)$.

Once the connection is obtained, the Riemann tensor can be calculated through

$$R^{\lambda}{}_{\rho\mu\nu} = \frac{\partial \Gamma^{\lambda}{}_{\nu\rho}}{\partial x^{\mu}} - \frac{\partial \Gamma^{\lambda}{}_{\mu\rho}}{\partial x^{\nu}} + \Gamma^{\lambda}{}_{\mu\sigma}\Gamma^{\sigma}{}_{\nu\rho} - \Gamma^{\lambda}{}_{\nu\sigma}\Gamma^{\sigma}{}_{\mu\rho}. \tag{A8}$$

It can also be treated as several 2-forms due to the antisymmetry of exchanging μ and ν,

$$\begin{aligned}\frac{1}{2}R^{\lambda}{}_{\rho\mu\nu}dx^{\mu}\wedge dx^{\nu} &= d\Gamma^{\lambda}{}_{\nu\rho}\wedge dx^{\nu} \\ &\quad + (\Gamma^{\lambda}{}_{\mu\sigma}dx^{\mu})\wedge(\Gamma^{\sigma}{}_{\nu\rho}dx^{\nu}).\end{aligned} \tag{A9}$$

In order to simplify the notation, label $\frac{1}{2}R^{\lambda}{}_{\rho\mu\nu}dx^{\mu}\wedge dx^{\nu}$ as $\Omega^{\lambda}{}_{\rho}$ and $\Gamma^{\lambda}{}_{\mu\sigma}dx^{\mu}$ as $A^{\lambda}{}_{\rho}$, then

$$\Omega^{\lambda}{}_{\rho} = dA^{\lambda}{}_{\rho} + A^{\lambda}{}_{\sigma}\wedge A^{\sigma}{}_{\rho}. \tag{A10}$$

These 1-forms $A^{\lambda}{}_{\rho}$ can be viewed as the connection 1-forms for the coordinates tetrad $(\partial_{\mu})^{\nu} = \delta^{\nu}{}_{\mu}$, while $\Omega^{\lambda}{}_{\rho}$ are their curvature 2-forms. Concretely, 1-forms $A^{\lambda}{}_{\rho}$ for the metric (3.1) are

$$\begin{aligned}&A^{a}{}_{b} = \bar{\Gamma}^{a}{}_{cb}du^{c} = \bar{A}^{a}{}_{b}, \\ &A^{a}_{i} = -(r\bar{\nabla}^{a}r)\hat{g}_{ij}dx^{j}, \qquad A^{i}{}_{a} = \frac{\bar{\nabla}_{a}r}{r}dx^{i}, \\ &A^{i}{}_{j} = \frac{\bar{\nabla}_{a}r}{r}\delta^{i}{}_{j}du^{a} + \hat{\Gamma}^{i}{}_{kj}dx^{k} = \frac{dr}{r}\delta^{i}{}_{j} + \hat{A}^{i}{}_{j}.\end{aligned} \tag{A11}$$

Then one obtains curvature 2-forms by applying Eq. (A10). First,

$$\Omega^{a}{}_{b} = dA^{a}{}_{b} + A^{a}{}_{c}\wedge A^{c}{}_{b} + A^{a}{}_{i}\wedge A^{i}{}_{b} = \bar{\Omega}^{a}{}_{b}, \tag{A12}$$

since term containing $\hat{g}_{ij}dx^i\wedge dx^j$ vanishes. Notice that

$$\Omega_{ai} = I_{ab}\Omega^{b}{}_{i} = -\Omega_{ia} = -r^2\hat{g}_{ij}\Omega^{j}{}_{a}, \tag{A13}$$

calculating $\Omega^{i}{}_{a}$ can avoid dealing with $d\hat{g}_{ij}$ here,

$$\Omega^{i}{}_{a} = \frac{\bar{\nabla}_{a}\bar{\nabla}_{b}r}{r}du^{b}\wedge dx^{i}. \tag{A14}$$

Therefore,

$$\Omega^{a}{}_{i} = -r\bar{\nabla}^{a}\bar{\nabla}_{b}r\hat{g}_{ij}du^{b}\wedge dx^{j}. \tag{A15}$$

The final 2-form $\Omega^{i}{}_{j}$ is

$$\Omega^i{}_j = \hat{\Omega}^i{}_j - I^{rr}\delta^i{}_k\hat{g}_{jl}dx^k \wedge dx^l$$
$$= \frac{1}{2}(\hat{R}^i{}_{jkl} - I^{rr}(\delta^i{}_k\hat{g}_{jl} - \delta^i{}_j\hat{g}_{jk}))dx^k \wedge dx^l, \quad \text{(A16)}$$

where the term I^{rr} is the short notation for $I^{ab}\bar{\nabla}_a r\bar{\nabla}_b r$. Remembering

$$dx^\mu \wedge dx^\nu = dx^\mu \otimes dx^\nu - dx^\nu \otimes dx^\mu, \quad \text{(A17)}$$

one can read the components of the Riemann tensor as

$$R^a{}_{bcd} = \bar{R}^a{}_{bcd},$$
$$R^a{}_{ibj} = -R^a{}_{ijb} = -r(\bar{\nabla}^a\bar{\nabla}_b r)\hat{g}_{ij},$$
$$R^i{}_{ajb} = -R^i{}_{abj} = -\frac{\bar{\nabla}_a\bar{\nabla}_b r}{r}\delta^i_j,$$
$$R^i{}_{jkl} = \hat{R}^i{}_{jkl} - I^{rr}(\delta^i{}_k\hat{g}_{jl} - \delta^i{}_j\hat{g}_{jk}). \quad \text{(A18)}$$

The same result can be found in Ref. [70]. Contracting $\delta^i_i = D - 2$, components of the Ricci tensor $R_{\mu\nu}$ are

$$R_{ab} = \bar{R}_{ab} - (D-2)\frac{\bar{\nabla}_a\bar{\nabla}_b r}{r},$$
$$R_{ij} = \hat{R}_{ij} - \hat{g}_{ij}(r\bar{\nabla}^2 r + (D-3)I^{rr}), \quad \text{(A19)}$$

in which the $\bar{\nabla}^2 r$ is $\bar{\nabla}^a\bar{\nabla}_a r$ for short. The Ricci scalar is

$$R = I^{ab}R_{ab} + \frac{\hat{g}^{ij}}{r^2}R_{ij}$$
$$= \bar{R} - 2(D-2)\frac{\bar{\nabla}^2 r}{r} + \frac{\hat{R}}{r^2} - (D-2)(D-3)\frac{I^{rr}}{r^2}. \quad \text{(A20)}$$

This paper further focuses on two-dimensional $\bar{\mathcal{M}}_{(2)}$. Since any two-dimensional metric is conformally flat (see [101,102]), the Einstein tensor of a two-dimensional metric always vanishes, i.e.,

$$\bar{R}_{ab} - \frac{\bar{R}}{2}I_{ab} = 0. \quad \text{(A21)}$$

In addition, we introduce $\mathcal{K} = \hat{R}/((D-2)(D-3))$ for simplicity [see Eq. (3.4)]. Therefore, the D-dimensional Einstein tensor $G_{\mu\nu}$ becomes

$$G_{ab} = -\frac{D-2}{r}\left(\bar{\nabla}_a\bar{\nabla}_b r - \frac{1}{2}I_{ab}\bar{\nabla}^2 r\right)$$
$$+ \frac{D-2}{2r}I_{ab}\left(\bar{\nabla}^2 r - \frac{D-3}{r}(\mathcal{K} - I^{rr})\right),$$
$$G_{ij} = \hat{R}_{ij} - (D-3)\mathcal{K}\hat{g}_{ij} - \hat{g}_{ij}\left(\frac{r^2}{2}\bar{R} - (D-3)r\bar{\nabla}^2 r\right.$$
$$\left. + \frac{(D-3)(D-4)}{2}(\mathcal{K} - I^{rr})\right), \quad \text{(A22)}$$

where we have separated the traceless part and trace part explicitly.

APPENDIX B: GENERAL EDDINGTON-FINKELSTEIN COORDINATES

The two-dimensional subspacetime must permit double null coordinates $\{u, v\}$ such that the line element becomes

$$ds^2 = -\Omega^2(u,v)dudv + r^2(u,v)\hat{g}_{ij}(x)dx^i dx^j. \quad \text{(B1)}$$

In the region where $\bar{\nabla}_a r$ does not vanish, r itself can be a coordinate, such that one can change to other coordinate frames like $\{v, r\}$. Since

$$dr = r_{,u}du + r_{,v}dv, \quad \text{(B2)}$$

where $r_{,u}$, $r_{,v}$ represents $\partial r/\partial u$, $\partial r/\partial v$, the line element becomes

$$ds^2 = \Omega^2\frac{r_{,v}}{r_{,u}}dv^2 - \frac{\Omega^2}{r_{,u}}drdv + r^2\hat{g}_{ij}(x)dx^i dx^j. \quad \text{(B3)}$$

The line element (B3) is still general. The coordinates frame $\{v, r\}$ is called general Eddington-Finkelstein (GEF) coordinates in this article. Define functions

$$\sigma(v,r) = -\frac{2}{\Omega^2}r_{,u},$$
$$f(v,r) = -\frac{4}{\Omega^2}r_{,u}r_{,v}, \quad \text{(B4)}$$

metric components under the GEF coordinates are

$$g_{vv} = I_{vv} = -\frac{f(v,r)}{\sigma^2(v,r)}, \qquad g_{rr} = I_{rr} = 0,$$
$$g_{vr} = g_{rv} = I_{vr} = I_{rv} = \frac{1}{\sigma(v,r)}, \qquad g_{ij} = r^2\hat{g}_{ij}, \quad \text{(B5)}$$

while inverse metric components are

$$g^{vv} = I^{vv} = 0, \qquad g^{rr} = I^{rr} = f(v,r),$$
$$g^{vr} = g^{rv} = I^{vr} = I^{rv} = \sigma(v,r), \qquad g^{ij} = \frac{\hat{g}^{ij}}{r^2}. \tag{B6}$$

In general, the shape of spacetime $\bar{\mathcal{M}}_{(2)} \times \hat{\mathcal{M}}_{(D-2)}$ with a given metric $\hat{g}_{ij}$ for the unit $\hat{\mathcal{M}}_{(D-2)}$ is described by two functions. In double null coordinates, they are $\Omega(u,v)$ and $r(u,v)$, while in GEF coordinates, they are $\sigma(v,r)$ and $f(v,r)$. The use of function $f(v,r)$ is convenient since it picks up the important function $I^{rr} = \nabla^\mu r \nabla_\mu r$. Further, the determinant of I_{ab} in the GEF coordinates is simply

$$I = -\frac{1}{\sigma^2}, \qquad \sqrt{-I} = \left|\frac{1}{\sigma}\right|. \tag{B7}$$

Therefore, the Laplacian of r in $\bar{\mathcal{M}}_{(2)}$ is

$$\bar{\nabla}^2 r = \sigma \frac{\partial(\sigma^{-1} I^{vr})}{\partial v} + \sigma \frac{\partial(\sigma^{-1} I^{rr})}{\partial r} = f' - \frac{\sigma'}{\sigma} f, \tag{B8}$$

where $'$ donates the derivative with respect to r. The result leads to the following simple expression:

$$\kappa_{\rm geo} = \frac{1}{2}\bar{\nabla}^2 r = \frac{f'}{2} - \frac{\sigma'}{\sigma}\frac{f}{2}, \tag{B9}$$

for the geometric surface gravity (3.60) in terms of f and σ. Then we will calculate the expansions of null vector fields tangent to $\bar{\mathcal{M}}_{(2)}$. Specify those null fields as

$$k^\mu \frac{\partial}{\partial X^\mu} = \frac{\partial}{\partial v} + \frac{f}{2\sigma}\frac{\partial}{\partial r}, \qquad l^\mu \frac{\partial}{\partial X^\mu} = -\sigma \frac{\partial}{\partial r}, \tag{B10}$$

which satisfy $k^\mu l_\mu = -1$. We assume that an increasing v indicates the future direction. Hence k^μ and l^μ are all future pointed. Their expansion can be easily calculated by the trick

$$\theta_{(k)} = \frac{D-2}{r} k^a \bar{\nabla}_a r = (D-2)\frac{f}{2\sigma r}, \tag{B11}$$

$$\theta_{(l)} = \frac{D-2}{r} l^a \bar{\nabla}_a r = -(D-2)\frac{\sigma}{r}, \tag{B12}$$

without dealing with $g^{\mu\nu}\nabla_\mu k_\nu$ and $g^{\mu\nu}\nabla_\mu l_\nu$. Such a method is also used in Ref. [68]. The hypersurface $I^{rr} = f = 0$ leads to $\theta_{(k)} = 0$, thus determining a trapping horizon, which is defined as a hypersurface foliated by marginal surfaces [51,66]. A marginal surface is a two-codimensional spatial surface with vanishing expansion. One can further classify types of trapping horizons according to the behavior of $\theta_{(l)}$ and $\mathcal{L}_l \theta_{(k)}$, see Refs. [51,66].

---

[1] J. D. Bekenstein, Generalized second law of thermodynamics in black hole physics, Phys. Rev. D **9**, 3292 (1974).
[2] J. M. Bardeen, B. Carter, and S. W. Hawking, The four laws of black hole mechanics, Commun. Math. Phys. **31**, 161 (1973).
[3] S. W. Hawking, Black holes and thermodynamics, Phys. Rev. D **13**, 191 (1976).
[4] J. M. Maldacena, The large N limit of superconformal field theories and supergravity, Adv. Theor. Math. Phys. **2**, 231 (1998).
[5] S. S. Gubser, I. R. Klebanov, and A. M. Polyakov, Gauge theory correlators from noncritical string theory, Phys. Lett. B **428**, 105 (1998).
[6] E. Witten, Anti–de Sitter space and holography, Adv. Theor. Math. Phys. **2**, 253 (1998).
[7] S. Ryu and T. Takayanagi, Holographic derivation of entanglement entropy from AdS/CFT, Phys. Rev. Lett. **96**, 181602 (2006).
[8] R. M. Wald, Black hole entropy is the Noether charge, Phys. Rev. D **48**, R3427 (1993).
[9] V. Iyer and R. M. Wald, Some properties of the Noether charge and a proposal for dynamical black hole entropy, Phys. Rev. D **50**, 846 (1994).
[10] S. W. Hawking, Black holes in general relativity, Commun. Math. Phys. **25**, 152 (1972).
[11] G. T. Horowitz and A. Strominger, Black strings and P-branes, Nucl. Phys. **B360**, 197 (1991).
[12] L. Vanzo, Black holes with unusual topology, Phys. Rev. D **56**, 6475 (1997).
[13] G. J. Galloway, K. Schleich, D. M. Witt, and E. Woolgar, Topological censorship and higher genus black holes, Phys. Rev. D **60**, 104039 (1999).
[14] R. Emparan and H. S. Reall, A rotating black ring solution in five dimensions, Phys. Rev. Lett. **88**, 101101 (2002).
[15] H. Elvang and P. Figueras, Black saturn, J. High Energy Phys. 05 (2007) 050.
[16] R. Emparan and H. S. Reall, Black holes in higher dimensions, Living Rev. Relativity **11**, 6 (2008).
[17] R. B. Mann, Pair production of topological anti-de Sitter black holes, Classical Quantum Gravity **14**, L109 (1997).
[18] D. Birmingham, Topological black holes in anti–de Sitter space, Classical Quantum Gravity **16**, 1197 (1999).
[19] R. Emparan, AdS/CFT duals of topological black holes and the entropy of zero energy states, J. High Energy Phys. 06 (1999) 036.
[20] D. Birmingham and S. Mokhtari, Stability of topological black holes, Phys. Rev. D **76**, 124039 (2007).
[21] D. Klemm, V. Moretti, and L. Vanzo, Rotating topological black holes, Phys. Rev. D **57**, 6127 (1998); **60**, 109902(E) (1999).

[22] T. Morley, P. Taylor, and E. Winstanley, Vacuum polarization on topological black holes, Classical Quantum Gravity **35**, 235010 (2018).
[23] X. Bai and J. Ren, Holographic Rényi entropies from hyperbolic black holes with scalar hair, J. High Energy Phys. 12 (2022) 038.
[24] M. Gutperle and A. Strominger, Space-like branes, J. High Energy Phys. 04 (2002) 018.
[25] G. Tasinato, I. Zavala, C. P. Burgess, and F. Quevedo, Regular S-brane backgrounds, J. High Energy Phys. 04 (2004) 038.
[26] H. Lu and J. F. Vazquez-Poritz, Nonsingular twisted S-branes from rotating branes, J. High Energy Phys. 07 (2004) 050.
[27] J. P. S. Lemos, Three dimensional black holes and cylindrical general relativity, Phys. Lett. B **353**, 46 (1995).
[28] R.-G. Cai and Y.-Z. Zhang, Black plane solutions in four-dimensional space-times, Phys. Rev. D **54**, 4891 (1996).
[29] S. A. Hartnoll, C. P. Herzog, and G. T. Horowitz, Building a holographic superconductor, Phys. Rev. Lett. **101**, 031601 (2008).
[30] S. A. Hartnoll, C. P. Herzog, and G. T. Horowitz, Holographic superconductors, J. High Energy Phys. 12 (2008) 015.
[31] T. Andrade and B. Withers, A simple holographic model of momentum relaxation, J. High Energy Phys. 05 (2014) 101.
[32] A. Donos and J. P. Gauntlett, Thermoelectric DC conductivities from black hole horizons, J. High Energy Phys. 11 (2014) 081.
[33] R. E. Arias and I. Salazar Landea, Thermoelectric transport coefficients from charged Solv and Nil black holes, J. High Energy Phys. 12 (2017) 087.
[34] W.-J. Jiang, H.-S. Liu, H. Lu, and C. N. Pope, DC conductivities with momentum dissipation in Horndeski theories, J. High Energy Phys. 07 (2017) 084.
[35] A. Esposito, S. Garcia-Saenz, A. Nicolis, and R. Penco, Conformal solids and holography, J. High Energy Phys. 12 (2017) 113.
[36] M. Baggioli and A. Buchel, Holographic viscoelastic hydrodynamics, J. High Energy Phys. 03 (2019) 146.
[37] A. Esposito, R. Krichevsky, and A. Nicolis, Solidity without inhomogeneity: Perfectly homogeneous, weakly coupled, UV-complete solids, J. High Energy Phys. 11 (2020) 021.
[38] M. Baggioli, K.-Y. Kim, L. Li, and W.-J. Li, Holographic axion model: A simple gravitational tool for quantum matter, Sci. China Phys. Mech. Astron. **64**, 270001 (2021).
[39] Y. Liu, X.-J. Wang, J.-P. Wu, and X. Zhang, Holographic superfluid with gauge-axion coupling, Eur. Phys. J. C **83**, 748 (2023).
[40] Y. Bardoux, M. M. Caldarelli, and C. Charmousis, Shaping black holes with free fields, J. High Energy Phys. 05 (2012) 054.
[41] Y. Tian, X.-N. Wu, and H.-B. Zhang, Holographic entropy production, J. High Energy Phys. 10 (2014) 170.
[42] Y. Tian, A topological charge of black holes, Classical Quantum Gravity **36**, 245001 (2019).
[43] Z. Y. Gao and L. Zhao, Restricted phase space thermodynamics for AdS black holes via holography, Classical Quantum Gravity **39**, 075019 (2022).
[44] T. Wang and L. Zhao, Black hole thermodynamics is extensive with variable Newton constant, Phys. Lett. B **827**, 136935 (2022).
[45] Z. Gao, X. Kong, and L. Zhao, Thermodynamics of Kerr-AdS black holes in the restricted phase space, Eur. Phys. J. C **82**, 112 (2022).
[46] L. Zhao, Thermodynamics for higher dimensional rotating black holes with variable Newton constant, Chin. Phys. C **46**, 055105 (2022).
[47] X. Kong, T. Wang, Z. Gao, and L. Zhao, Restricted phased space thermodynamics for black holes in higher dimensions and higher curvature gravities, Entropy **24**, 1131 (2022).
[48] T. Wang, Z. Zhang, X. Kong, and L. Zhao, Topological black holes in Einstein-Maxwell and 4D conformal gravities revisited, Nucl. Phys. **B995**, 116352 (2023).
[49] M. R. Visser, Holographic thermodynamics requires a chemical potential for color, Phys. Rev. D **105**, 106014 (2022).
[50] C. W. Misner and D. H. Sharp, Relativistic equations for adiabatic, spherically symmetric gravitational collapse, Phys. Rev. **136**, B571 (1964).
[51] S. A. Hayward, Gravitational energy in spherical symmetry, Phys. Rev. D **53**, 1938 (1996).
[52] H. Kodama, Conserved energy flux for the spherically symmetric system and the backreaction problem in the black hole evaporation, Prog. Theor. Phys. **63**, 1217 (1980).
[53] K.-i. Nakao, C.-M. Yoo, and T. Harada, Gravastar formation: What can be the evidence of a black hole?, Phys. Rev. D **99**, 044027 (2019).
[54] G. Hütsi, T. Koivisto, M. Raidal, V. Vaskonen, and H. Veermäe, Cosmological black holes are not described by the Thakurta metric: LIGO-Virgo bounds on PBHs remain unchanged, Eur. Phys. J. C **81**, 999 (2021).
[55] T. Harada, H. Maeda, and T. Sato, Thakurta metric does not describe a cosmological black hole, Phys. Lett. B **833**, 137332 (2022).
[56] C.-M. Yoo, T. Harada, S. Hirano, H. Okawa, and M. Sasaki, Primordial black hole formation from massless scalar isocurvature, Phys. Rev. D **105**, 103538 (2022).
[57] T. Sato, H. Maeda, and T. Harada, Conformally Schwarzschild cosmological black holes, Classical Quantum Gravity **39**, 215011 (2022).
[58] A. Escrivà, Y. Tada, S. Yokoyama, and C.-M. Yoo, Simulation of primordial black holes with large negative non-Gaussianity, J. Cosmol. Astropart. Phys. 05 (2022) 012.
[59] J.-R. Ren and R. Li, Unified first law and thermodynamics of dynamical black hole in n-dimensional Vaidya spacetime, Mod. Phys. Lett. A **23**, 3265 (2008).
[60] K. X. Jiang, S. M. Ke, and D. T. Peng, Hawking radiation as tunneling and the unified first law of thermodynamics for a class of dynamical black holes, Int. J. Mod. Phys. D **18**, 1707 (2009).
[61] R. Di Criscienzo, S. A. Hayward, M. Nadalini, L. Vanzo, and S. Zerbini, Hamilton-Jacobi tunneling method for dynamical horizons in different coordinate gauges, Classical Quantum Gravity **27**, 015006 (2010).

[62] R. di Criscienzo, M. Nadalini, L. Vanzo, S. Zerbini, and S. Hayward, Invariance of the tunneling method for dynamical black holes, in *12th Marcel Grossmann Meeting on General Relativity* (World Scientific, Singapore, 2010), pp. 1166–1168.
[63] L. Vanzo, G. Acquaviva, and R. Di Criscienzo, Tunnelling methods and Hawking's radiation: Achievements and prospects, Classical Quantum Gravity **28**, 183001 (2011).
[64] S.-B. Kong, H. Abdusattar, Y. Yin, H. Zhang, and Y.-P. Hu, The $P-V$ phase transition of the FRW universe, Eur. Phys. J. C **82**, 1047 (2022).
[65] H. Abdusattar, S.-B. Kong, Y. Yin, and Y.-P. Hu, The Hawking-Page-like phase transition from FRW spacetime to McVittie black hole, J. Cosmol. Astropart. Phys. 08 (2022) 060.
[66] S. A. Hayward, Unified first law of black hole dynamics and relativistic thermodynamics, Classical Quantum Gravity **15**, 3147 (1998).
[67] R.-G. Cai and S. P. Kim, First law of thermodynamics and Friedmann equations of Friedmann-Robertson-Walker universe, J. High Energy Phys. 02 (2005) 050.
[68] R.-G. Cai and L.-M. Cao, Unified first law and thermodynamics of apparent horizon in FRW universe, Phys. Rev. D **75**, 064008 (2007).
[69] H. Zhang, S. A. Hayward, X.-H. Zhai, and X.-Z. Li, Schwarzschild solution as a result of thermodynamics, Phys. Rev. D **89**, 064052 (2014).
[70] H. Maeda and M. Nozawa, Generalized Misner-Sharp quasilocal mass in Einstein-Gauss-Bonnet gravity, Phys. Rev. D **77**, 064031 (2008).
[71] H. Zhang, Y. Hu, and X.-Z. Li, Misner-Sharp mass in n-dimensional $f(R)$ gravity, Phys. Rev. D **90**, 024062 (2014).
[72] Y.-P. Hu and H. Zhang, Misner-Sharp mass and the unified first law in massive gravity, Phys. Rev. D **92**, 024006 (2015).
[73] H.-W. Tan, J.-B. Yang, T.-M. He, and J.-Y. Zhang, A modified thermodynamics method to generate exact solutions of Einstein equations, Commun. Theor. Phys. **67**, 41 (2017).
[74] S. Kinoshita, Extension of Kodama vector and quasilocal quantities in three-dimensional axisymmetric spacetimes, Phys. Rev. D **103**, 124042 (2021).
[75] G. Dotti and R. J. Gleiser, Obstructions on the horizon geometry from string theory corrections to Einstein gravity, Phys. Lett. B **627**, 174 (2005).
[76] H. Maeda, Gauss-Bonnet black holes with nonconstant curvature horizons, Phys. Rev. D **81**, 124007 (2010).
[77] S. Ray, Birkhoff's theorem in Lovelock gravity for general base manifolds, Classical Quantum Gravity **32**, 195022 (2015).
[78] S. Ohashi and M. Nozawa, Lovelock black holes with a nonconstant curvature horizon, Phys. Rev. D **92**, 064020 (2015).
[79] H. Zhang and X.-Z. Li, From thermodynamics to the solutions in gravity theory, Phys. Lett. B **737**, 395 (2014).
[80] Y.-P. Hu, X.-M. Wu, and H. Zhang, Generalized Vaidya solutions and Misner-Sharp mass for n-dimensional massive gravity, Phys. Rev. D **95**, 084002 (2017).
[81] D. R. Brill, J. Louko, and P. Peldan, Thermodynamics of $(3+1)$-dimensional black holes with toroidal or higher genus horizons, Phys. Rev. D **56**, 3600 (1997).
[82] S. Song, H. Li, Y. Ma, and C. Zhang, Entropy of black holes with arbitrary shapes in loop quantum gravity, Sci. China Phys. Mech. Astron. **64**, 120411 (2021).
[83] J. Ren, Analytic solutions of neutral hyperbolic black holes with scalar hair, Phys. Rev. D **106**, 086023 (2022).
[84] W. Hawking and G. F. R. Ellis, *The Large Scale Structure of Space-Time* (Cambridge University Press, Cambridge, England, 1973), 10.1017/CBO9780511524646.
[85] S. A. Hayward, General laws of black hole dynamics, Phys. Rev. D **49**, 6467 (1994).
[86] Z.-F. Mai and R.-Q. Yang, Black holes as rechargeable batteries and nuclear reactors, Phys. Rev. D **108**, 104066 (2023).
[87] H. Maeda and C. Martinez, All static and electrically charged solutions with Einstein base manifold in the arbitrary-dimensional Einstein-Maxwell system with a massless scalar field, Eur. Phys. J. C **78**, 860 (2018).
[88] Y. Peng, New topological Gauss-Bonnet black holes in five dimensions, Phys. Rev. D **104**, 084004 (2021).
[89] Y. Peng, New anisotropic Gauss-Bonnet black holes in five dimensions at the critical point, Eur. Phys. J. C **84**, 81 (2024).
[90] H. Maeda, The Roberts–(A)dS spacetime, Classical Quantum Gravity **32**, 135025 (2015).
[91] H. Huang, Z.-Y. Fan, and H. Lü, Static and dynamic charged black holes, Eur. Phys. J. C **79**, 975 (2019).
[92] H. Huang, H. Lü, and J. Yang, Bronnikov-like wormholes in Einstein-scalar gravity, Classical Quantum Gravity **39**, 185009 (2022).
[93] C. Gundlach, P. Bourg, and A. Davey, Fully constrained, high-resolution shock-capturing, formulation of the Einstein-fluid equations in $2+1$ dimensions, Phys. Rev. D **104**, 024061 (2021).
[94] J. D. Brown and J. W. York, Jr., Quasilocal energy and conserved charges derived from the gravitational action, Phys. Rev. D **47**, 1407 (1993).
[95] M. M. Caldarelli, G. Cognola, and D. Klemm, Thermodynamics of Kerr-Newman-AdS black holes and conformal field theories, Classical Quantum Gravity **17**, 399 (2000).
[96] S. Chakraborty and T. Padmanabhan, Thermodynamical interpretation of the geometrical variables associated with null surfaces, Phys. Rev. D **92**, 104011 (2015).
[97] S. Chakraborty, K. Parattu, and T. Padmanabhan, Gravitational field equations near an arbitrary null surface expressed as a thermodynamic identity, J. High Energy Phys. 10 (2015) 097.
[98] S. Mahapatra, S. Priyadarshinee, G. N. Reddy, and B. Shukla, Exact topological charged hairy black holes in AdS Space in d-dimensions, Phys. Rev. D **102**, 024042 (2020).
[99] S. Priyadarshinee, S. Mahapatra, and I. Banerjee, Analytic topological hairy dyonic black holes and thermodynamics, Phys. Rev. D **104**, 084023 (2021).
[100] M. Guica, T. Hartman, W. Song, and A. Strominger, The Kerr/CFT correspondence, Phys. Rev. D **80**, 124008 (2009).
[101] R. Wald, *General Relativity* (The University of Chicago, Chicago and London, 1984).
[102] C.-B. Liang and B. Zhou, *Differential Geometry and General Relativity* (Springer, Singapore, 2023).